Thermodynamic properties of carbon-phenolic gas mixtures

James B. Scoggins[a,*], Jason Rabinovich[b,1], Benjamin Barros-Fernandez[a,2], Alexandre Martin[c], Jean Lachaud[d], Richard L. Jaffe[e], Nagi N. Mansour[f], Guillaume Blanquart[b], Thierry E. Magin[a]

[a] *Aeronautics and Aerospace Department, von Karman Institute for Fluid Dynamics, B-1640 Rhode-St-Genèse, Belgium*
[b] *Department of Mechanical Engineering, California Institute of Technology, Pasadena, California, 91125*
[c] *Department of Mechanical Engineering, University of Kentucky, Lexington, KY, 40506*
[d] *University of California Santa Cruz, Silicon Valley Initiatives, Moffett Field, CA, 94035*
[e] *Aerothermodynamics Branch, Entry Systems Division, NASA Ames Research Center, Moffett Field, CA, 94035*
[f] *Computational Physics Branch, NASA Advanced Supercomputing Division, NASA Ames Research Center, Moffett Field, CA, 94035*

Abstract

Accurate thermodynamic properties for species found in carbon-phenolic gas mixtures are essential in predicting material response and heating of carbon-phenolic heat shields of planetary entry vehicles. A review of available thermodynamic data for species found in mixtures of carbon-phenolic pyrolysis and ablation gases and atmospheres rich with C, H, O, and N such as those of Earth, Mars, Titan, and Venus, is performed. Over 1200 unique chemical species are identified from four widely used thermodynamic databases and a systematic procedure is described for combining these data into a comprehensive model. The detailed dataset is then compared with the Chemical Equilibrium with Applications thermodynamic database developed by NASA in order to quantify the differences in equilibrium thermodynamic properties obtained with the two databases. In addition, a consistent reduction methodology using the mixture thermodynamic properties as an objective function is developed to generate reduced species sets for a variety of temperature, pressure, and elemental composition spaces. It is found that 32 and 23 species are required to model carbon-phenolic pyrolysis gases mixed with air and CO_2, respectively, to maintain a maximum error in thermodynamic quantities below 10 %.

Keywords: thermodynamics, ablation, pyrolysis, carbon-phenolic, thermal protection materials, re-entry vehicles

Nomenclature

$\mathcal{A}$	= ordered species set with decreasing Θ	B	= stoichiometry matrix
a	= sound speed, $\mathrm{m\,s^{-1}}$	B'	= nondimensional mass flux

*Corresponding author
[1] Now at Jet Propulsion Laboratory
[2] Now at Airbus

C_M = Stanton number

C_p = molar specific heat at constant pressure, $\mathrm{J\,mol^{-1}\,K^{-1}}$

c_p = specific heat at constant pressure per mass, $\mathrm{J\,kg^{-1}\,K^{-1}}$

c_v = specific heat at constant volume per mass, $\mathrm{J\,kg^{-1}\,K^{-1}}$

e = energy per mass, $\mathrm{J\,kg^{-1}}$

G = Gibbs free energy, $\mathrm{J\,mol^{-1}}$

H = molar enthalpy, $\mathrm{J\,mol^{-1}}$

h = enthalpy per mass, $\mathrm{J\,kg^{-1}}$

M = molecular weight, $\mathrm{kg\,mol^{-1}}$

$\dot{m}$ = mass flux, $\mathrm{kg\,s^{-1}\,m^{-2}}$

N = moles, mol

P = (T, p, x^e) point

p = pressure, Pa

$\mathcal{R}$ = reduction space

R_j = species gas constant, R_u/M_j

R_u = universal gas constant, $8.314\,\mathrm{J\,mol^{-1}\,K^{-1}}$

S = entropy, $\mathrm{J\,mol^{-1}\,K^{-1}}$

s = entropy, $\mathrm{J\,kg^{-1}\,K^{-1}}$

$\dot{s}$ = recession rate, $\mathrm{m\,s^{-1}}$

T = temperature, K

Θ = thermodynamic error function

u = velocity, $\mathrm{m\,s^{-1}}$

x = mole fraction

y = mass fraction

χ = char yield

$\mathcal{E}$ = set of element indices

γ = specific heat ratio, c_p/c_v

γ_s = isentropic exponent

ρ = density, $\mathrm{kg\,m^{-3}}$

$\mathcal{S}$ = set of species indices

Subscripts

c = char

e = boundary layer edge

g = pyrolysis gas

i, k = element

j = species

r = reduction space

s = species subset

w = wall

Superscripts

e = elemental quantity

resin = resin quantity

s = computed using species in $\mathcal{S}_s$

$\circ$ = evaluated at standard-state p

Acronyms

ATcT = Active Thermochemical Tables

CEA = Chemical Equilibrium with Applications

JANAF = Joint-Army-Navy-air Force

NASA = National Aeronautics and Space Administration

NIST = National Institute of Standards and Technology

PAH = polycyclic aromatic hydrocarbons

PICA = phenolic impregnated carbon ablator

TN = thermochemical network

TPS = thermal protection system

1. Introduction

In the wake of the Apollo program and multiple atmospheric entries on other planets and moons, the next two space exploration challenges, in terms of aerothermodynamics, are robotic sample return missions and the human exploration of Mars. Many achievements in atmospheric entry science have been made since the 1960's, but prediction of the heat flux at the surface of the spacecraft remains an imperfect art.

Ablative thermal protection systems (TPS), like those recently used on the successful Mars Science Laboratory (MSL) and Stardust missions, dissipate the extreme convective and radiative heat fluxes imposed on hypersonic entry vehicles through thermal decomposition of the thermal protection material (TPM). Ablative TPMs have also been used in the design of solid rocket nozzles to protect the nozzle walls from the high temperature gaseous combustion products. A specific class of lightweight, composite ablators were developed at NASA Ames Research Center (ARC) in the 1990's in an effort to improve on the existing TPMs [1, 2]. In general, these materials are composed of low density, fibrous carbon substrates impregnated with an organic, polymeric resin. Examples designed for high-enthalpy atmospheric entry include phenolic impregnated carbon ablator (PICA, developed at NASA ARC in the 1990's and first used on the Stardust forebody heat shield, launched in 1999) [1–3], ASTERM (a PICA-like material under development by Astrium through ESA, starting in the early 2000's) [4], and PICA-X[3] (a PICA-like material developed by NASA for SpaceX). Sharpe and Wright [5] provide a review of materials used for applications in extreme environments from the 1960's until the present.

The accurate characterization and modeling of these TPMs is crucial for the safe design of TPSs and rocket nozzles. Although this has been an active field of research since the 1960s [6–19], state of the art modeling tools used for high-enthalpy aerothermodynamic predictions leave room for improvement, and prediction uncertainties remain as high as 60 % for laminar convective heating [20–23]. These uncertainties force TPS designers to include significant safety factors when determining the TPS thickness, adding unnecessary mass to the vehicle design which in turn increases propellant mass and decreases mass available for scientific payloads.

Ablation phenomena have been described previously in great detail, and many of the modeling issues and uncertainties that are associated with ablation have been reviewed in previous works [24–33] and are summarized below. In general, the virgin TPM is primarily affected by two physical phenomena. The first, known as pyrolysis, refers to the thermal decomposition of a phenolic resin. At high temperatures, phenolic resin is progressively carbonized into a lower density carbon, known as char. Approximately 50% of the resins' original mass is converted to the gas phase [16, 34]. Pyrolysis gases are then transported out of the heatshield by diffusion and convection through the porous carbon fiber substrate. The chemical composition

[3] PICA Heat shield, http://www.spacex.com/news/2013/04/04/pica-heat-shield, accessed May 4, 2016.

of the high temperature pyrolysis gas evolves as it flows through the porous carbon fiber structure, and will eventually mix and continue to react with the surface ablation products and the atmospheric gases.

The second phenomenon, surface ablation, refers to mass removal in a thin volumetric layer of carbon fibers near the surface of the heatshield through heterogeneous chemical processes, including oxidation, nitridation, and sublimation. Surface ablation occurs in both non-charring materials, such as carbon/carbon ablators, and in charring ablators, such as carbon-phenolics. Charring ablators will be focused on in this work.

Determining the chemical composition of the gas close to the surface of an ablative heatshield is necessary to accurately predict the surface heat flux. Many material response codes assume that the gas mixture near the surface of the heatshield is in thermodynamic equilibrium (see [35] for a summary of ablation code capabilities), and this paper will remain consistent with that assumption. An analysis of finite-rate kinetics related to the gas mixture is outside of the scope of this work. Equilibrium compositions are dependent entirely on the underlying thermodynamic data for the species considered. To the authors' knowledge, a detailed review of thermodynamic data for carbon-phenolic gases has never been performed and no consensus exists concerning which species should be considered in these mixtures.

The primary goals of this work are to a) provide a detailed review of available thermodynamic data for species relevant to the simulation of the material response of carbon-phenolic TPMs, subjected to high-enthalpy flows, b) compile a detailed thermodynamic database based on this review, and c) develop reduced species sets suitable for the accurate calculation of mixture thermodynamic properties over the range of temperatures, pressures, and elemental compositions of interest to TPS designers. The paper is organized in several parts. In the following section, a review of experimental and theoretical elemental compositions relevant to carbon-phenolic TPMs is performed in order to define the elemental composition space of interest in this work. Next, a review of thermodynamic data sources is presented along with a methodology for combining each data source to form an extensive thermodynamic database for carbon phenolic-gases, placing an emphasis on the consistency and quality of the data. The database is then compared to the commonly used CEA [36] database and the relevant differences are discussed. Finally, a novel species reduction procedure is presented and used to create several reduced species sets which are guaranteed to provide accurate mixture thermodynamic properties over the entire temperature, pressure, and elemental composition space of interest.

2. Constraints on the Thermodynamic Database

In this work, we have limited the set of species considered to those which contain the elements C, H, O, and N, because of their relevance to typical atmospheric ablation problems. The addition of minor species such as Ar or Si compounds will not be considered here in an effort to limit the scope of this work. In this section we discuss other constraints placed on the database, including the necessary thermodynamic properties and elemental composition space.

2.1. Equilibrium Thermodynamic Properties

For a gas phase mixture composed of the species in set $\mathcal{S}$, the total molar Gibbs energy is defined as

$$G \equiv \sum_{j \in \mathcal{S}} x_j \Big(H_j(T) - T S_j^\circ(T) + R_u T \ln \frac{p_j}{p^\circ} \Big), \tag{1}$$

where x_j, $p_j = x_j p$, H_j, and S_j° are respectively the mole fraction, partial pressure, molar enthalpy, and molar standard state entropy of species j. For a given temperature T, pressure p, and elemental mole fractions x_i^e, the equilibrium composition of a gas mixture is determined when Eq. 1 is minimized according to the following mass balance constraints,

$$\frac{N}{N^e} \sum_{j \in \mathcal{S}} B_{ji} x_j = x_i^e, \quad \forall\, i \in \mathcal{E}, \tag{2}$$

where B_{ji} represents the number of atoms of element i belonging to species j. Using the Lagrange multiplier technique, the constrained minimization problem is easily converted to a nonlinear system of the form

$$x_j = \exp\Big(- H_j(T) + T S_j^\circ(T) - R_u T \ln \frac{p}{p^\circ} + \sum_{i \in \mathcal{E}} \lambda_i B_{ji} \Big), \quad \forall\, j \in \mathcal{S}, \tag{3}$$

where the Lagrange multipliers, λ_i, have been introduced. Substituting Eq. 3 into Eq. 2, and enforcing that species mole fractions sum to unity, yields a nonlinear system of $n^{\mathcal{E}} + 1$ equations and as many unknowns. This system can then be stably solved via the Gibbs function continuation method developed by Pope [37] and recently generalized to any number of ideal phases by Scoggins and Magin [38].

Typically, mixture thermodynamic properties are most readily used on a per mass basis. For a given equilibrium composition, the mixture enthalpy, entropy, and energy per mass are

$$h = \sum_{j \in \mathcal{S}} y_j h_j(T), \tag{4}$$

$$s = \sum_{j \in \mathcal{S}} y_j \Big[s_j^\circ(T) - R_j \ln \frac{p_j}{p^\circ} \Big], \quad \text{and} \tag{5}$$

$$e = h - \frac{p}{\rho}, \tag{6}$$

respectively, where the mixture density is given by the Ideal Gas Law, $\rho = pM/R_u T$, and $M = \sum_{j \in \mathcal{S}} x_j M_j$ is the mixture molecular weight. Mixture specific heats are defined as

$$c_p \equiv \Big(\frac{\partial h}{\partial T} \Big)_p = \sum_{j \in \mathcal{S}} y_j c_{p,j} + \sum_{j \in \mathcal{S}} h_j \Big(\frac{\partial y_j}{\partial T} \Big)_p, \tag{7}$$

$$c_v \equiv \Big(\frac{\partial e}{\partial T} \Big)_v = c_p + \left[\frac{p}{\rho^2} - \Big(\frac{\partial e}{\partial p} \Big)_T \Big(\frac{\partial p}{\partial \rho} \Big)_T \right] \Big(\frac{\partial \rho}{\partial T} \Big)_p. \tag{8}$$

The first summation in Eq. 7 is referred to as the mixture "frozen" specific heat because it is the c_p of a frozen mixture, whose composition is fixed. The second summation is named the "reactive" c_p as it accounts

for the change in the composition with respect to temperature through reactions at equilibrium [39]. Note that the mass fraction derivatives in Eq. 7 may be obtained analytically by relating them to mole fraction derivatives and differentiating Eq. 3. The partial derivatives on the right hand side of Eq. 8 are readily obtained by differentiating Eq. 6 along with the Ideal Gas Law. The equilibrium speed of sound is

$$a^2 = \left(\frac{\partial p}{\partial \rho}\right)_s = \gamma \left(\frac{\partial \rho}{\partial p}\right)_T^{-1} = \gamma_s \frac{p}{\rho}, \tag{9}$$

where $\gamma = c_p/c_v$ is the equilibrium specific heat ratio and γ_s is the isentropic exponent.

Finally, pure species enthalpies and entropies are related to their specific heats via the molar thermodynamic relations

$$H_j(T) = \int_{T^\circ}^{T} C_{p,j}(T) dT + H_j(T^\circ), \tag{10}$$

$$S_j^\circ(T) = \int_{T^\circ}^{T} \frac{C_{p,j}(T)}{T} dT + S_j^\circ(T^\circ). \tag{11}$$

Therefore, at a minimum, a thermodynamic database must provide species specific heats at constant pressure, $C_{p,j}(T)$, and the standard-state species enthalpies and entropies from Eq. 10 and Eq. 11. With that information, the equilibrium species mole fractions can be determined by minimizing the Gibbs free energy of the system, given temperature and pressure and an elemental composition, which allows the computation of mixture equilibrium thermodynamic properties.

2.2. Elemental Composition Space

As described in the previous section, the thermodynamic properties of a mixture in local thermodynamic equilibrium (LTE) strongly depend on the elemental composition of the mixture. For gases flowing in and around an ablating and pyrolyzing carbon-phenolic TPM during atmospheric entry, the local elemental composition depends strongly on the time-dependent material response of the ablator and trajectory of the entry vehicle. In general, the elemental composition of the gas will be a mixture of the atmosphere and pyrolysis and ablation product compositions.

2.2.1. Atmospheric Compositions

In this work, only the atmospheres of Earth, Mars, Venus, and Titan are considered since their elemental compositions are dominated by carbon, hydrogen, oxygen, and nitrogen. Table 1 provides a summary of the species and element compositions (by mole) for each of these atmospheres. Note that Mars and Venus are both nearly 96 % CO_2 by mole, indicating that their equilibrium thermodynamic properties may be approximated by a pure CO_2 gas. Similarly, Titan's atmosphere is mostly (98 %) N_2, allowing it to be approximated by a pure N_2 gas. While these approximations are sufficient for describing the mixture equilibrium thermodynamic properties of these atmospheres, they may not be sufficient for describing other phenomena of interest such as radiative heat transport. However, such phenomena are beyond the scope of this work and are not considered here.

Table 1: Nominal molar compositions of major species and elements for the atmospheres considered in this work.

Atmosphere	Percentage of Major Species						Element Fractions[a]				Ref.
	N_2	O_2	CO_2	CH_4	H_2	Ar	C	H	O	N	
Earth	78.1	20.9	-	-	-	0.9	-	-	0.211	0.789	[40]
Mars	1.9	-	95.9	-	-	2.0	0.327	-	0.653	0.020	[40]
Titan	98.4	-	-	1.4	0.2	-	0.007	0.029	-	0.964	[41]
Venus	3.5	-	96.5	-	-	-	0.325	-	0.651	0.024	[40]

[a] Ar element fractions have been added to N

2.2.2. Pyrolysis and Ablation Product Compositions

The pyrolysis gases formed during the thermal decomposition of a phenolic resin are strongly dependent on the molecular structure of the original polymer and the local temperature at which decomposition occurs. A recent review of the thermal decomposition process has been made by Rabinovitch [42] and is summarized here. Phenolic resins are generally formed through a polycondensation reaction which occurs when a combination of phenol (C_6H_5OH) and formaldehyde (CH_2O) are heated in the presence of a catalyst. When excess formaldehyde is present in the mixture, a basic (alkaline) catalyst is used to promote cross-linking of the polymer through ethylene bridges, forming a novolac resin. When there is an excess of phenol, a resole type resin is produced in the presence of an acidic catalyst. Depending on the formaldehyde to phenol ratio, reaction temperature, catalyst, reaction time, and distillation amount, a wide variety of phenolic resin structures may be obtained, with various degrees of cross-linking and impurities. Fig. 1 shows the polymer structure of two idealized examples of a phenolic resin (without impurities) that may be produced. The linear polymer represents a minimal amount of cross-linking and has a repeated stoichiometry of C_7H_6O, while the fully cross-linked polymer can be characterized by a stoichiometry of $C_{15}H_{12}O_2$. Typical polymer structures fall somewhere in between these idealized cases due to incomplete cross-linking and the presence of impurities embedded in the resin, such as nitrogen [43].

A significant number of experimental studies have been performed to characterize the thermal decomposition of various types of carbon-phenolic resins and TPS. In particular, several important studies have measured the composition of the pyrolysis gases produced versus temperature for various materials, including novolac [16] and resol [44] resins, carbon-phenolic [45], and PICA [46, 47]. Fig. 2a compares the elemental pyrolysis gas compositions versus temperature measured in these studies. While some variability in the compositions exists, the thermal decomposition of a phenolic resin can generally be described in three temperature regimes. Between 300 °C to 600 °C, small molecules which are not linked to the bulk polymer (left over from resin formation) are allowed to escape. In addition, ether and nitrogen linkages begin to break, forming a mixture of aldehydes, cresols, and azomethines. The most significant pyrolysis gas formed in this stage is typically water. From 600 °C to 900 °C, the bulk of the pyrolysis gases are formed. A

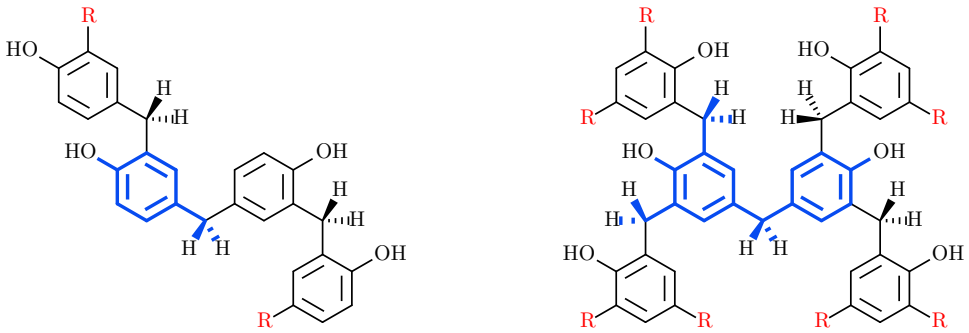

(a) Linearly-linked resin (C_7H_6O).

(b) Fully-linked resin ($C_{15}H_{12}O_2$).

Figure 1: Molecular structures of idealized phenolic resins. Blue bond-lines indicate the repeated structure in the resin and "R" indicates the structure repeats.

significant shrinkage of the polymer occurs due to the creation of carbon-carbon bonds between aromatic rings, forming a polyaromatic char. Several gases may be formed in this range, such as H_2, CH_4, H_2O, CO, CO_2, and volatile aromatics such as phenol (C_6H_5OH) and benzene (C_6H_6). Finally, above about 900 °C, dehydrogenation further shrinks the polymer forming mostly H_2 and other small noncarbonacious molecules.

The formation of the polyaromatic char during the pyrolysis of a phenolic resin ensures that the pyrolysis gas composition is not the same as the composition of the virgin resin. In addition, because the pyrolysis process occurs in several stages, the pyrolysis gas composition is not expected to be constant throughout the TPS material. Nevertheless, it is often sufficient to assume that the char is composed purely of carbon atoms [30] and treat pyrolysis as a single step reaction of the form:

$$\mathrm{C_aH_bO_c\ (resin)} \xrightarrow{\text{pyrolysis}} \mathrm{C_\alpha H_b O_c\ (gas)} + \mathrm{C_{(a-\alpha)}\ (char)}, \tag{12}$$

where the amount of carbon produced in the gas phase is related to the total char yield χ of the reaction via,

$$\alpha(\chi) = \mathrm{a}\big(1 - \frac{\chi}{y_{\mathrm{C}}^{\mathrm{resin}}}\big), \quad y_{\mathrm{C}}^{\mathrm{resin}} = \frac{\mathrm{a}M_{\mathrm{C}}}{\mathrm{a}M_{\mathrm{C}} + \mathrm{b}M_{\mathrm{H}} + \mathrm{c}M_{\mathrm{O}}}. \tag{13}$$

The char yield of a given resin is defined simply as

$$\chi \equiv \frac{\text{mass of charred resin}}{\text{mass of virgin resin}}. \tag{14}$$

The condition that $\alpha(\chi) \geq 0$ implies the maximum char yield for any resin (assuming a pure carbon char) is the carbon mass fraction in the virgin resin, $0 \leq \chi \leq y_{\mathrm{C}}^{\mathrm{resin}}$. Therefore, the theoretical maximum char yields of linear and fully-linked polymers (see Fig. 1) are 79.2 % and 80.4 % respectively. Typical char yields of real carbon-phenolic TPS materials range between 50 % to 65 %. For example, the elemental mole fractions of $\{\mathrm{C} : \mathrm{H} : \mathrm{O}\} = \{0.229 : 0.661 : 0.110\}$ have been used extensively to model the pyrolysis gas from carbon-

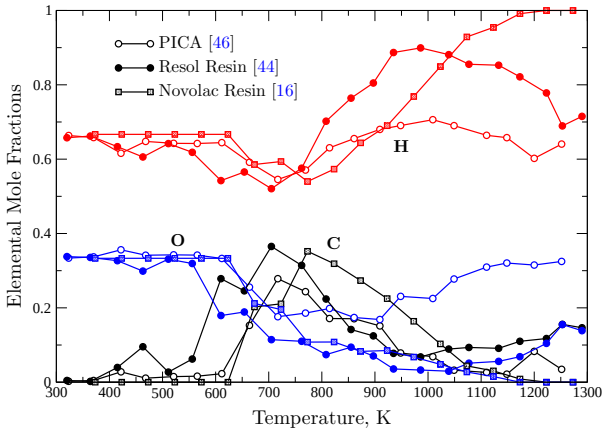

(a) Experimentally determined pyrolysis gas compositions versus temperature for various materials. Elemental compositions have been computed based on species data reported in [16, 44, 46].

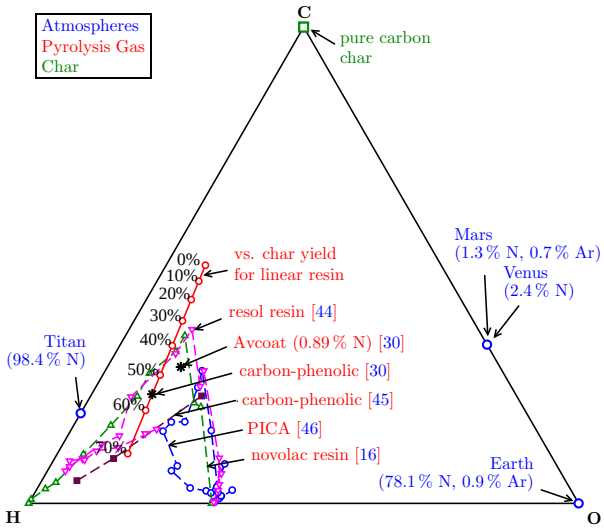

(b) Compositions projected onto the C-H-O mole fraction plane. When other elements belong to a composition, they are given in parentheses.

Figure 2: Summary of elemental compositions for various atmospheres and experimental and theoretical pyrolysis gas and char compositions.

phenolic TPS materials which corresponds to a char yield of 50 % for pure phenol (C_6H_5OH) or about 56 % for a linear resin [30, 48, 49].

2.2.3. Effect of Mixing

A summary of the various atmospheric and pyrolysis and ablation product compositions discussed above is given in Fig. 2. Fig. 2b provides a 2-dimensional representation of each composition by projecting them onto the C-H-O mole fraction simplex plane, based on the constraint that the mole fractions sum to unity. The closer a composition is to one of the vertices of the simplex, the more that composition consists of the element at that vertex. For example, the compositions of the Martian and Venusian atmospheres are close to that of CO_2. Consequently, those compositions lie on the edge of the simplex connecting C and O, and the distance to O is half the distance to C.

In reality, the local elemental composition for flows in and around a carbon-phenolic TPS material will result from the mixing of the pyrolysis gases, ablation products, and atmospheric gases. When two gases with different compositions are mixed, the mixture composition will lie on a line between one of the compositions in Fig. 2b. From the figure, it is therefore clear that nearly the entire C-H-O simplex represents the feasible region of compositions. Furthermore, because the atmospheres of Titan and Earth are mostly nitrogen gas, we may also assume that the entire range of nitrogen mole fractions are possible as well. Indeed, many experimental investigations use pure nitrogen test gases to limit oxidation at the surface of the material or to simplify numerical simulations of the experiments. For these reasons, an equilibrium thermodynamic

database must be valid over the entire C-H-O-N composition space.

3. Thermodynamic Database Compilation

3.1. Review of Available Thermodynamic Data

Before presenting the compilation of thermodynamic data, a short review of the publicly available data used in this work is presented. The data sources below are widely available and have been used extensively in the literature. This, however, should not be considered an exhaustive list.

One of the most commonly used data sources is the NASA 9-coefficient polynomial database of Gordon and McBride [36, 50–52] provided with the NASA Chemical Equilibrium and Applications (CEA) program [53, 54]. In total, the CEA database provides thermodynamic data for 193 gaseous species containing the elements C, H, O, and N. The data for the majority of the species are provided by calculations made at NASA Glenn Research Center by Gordon and McBride. The remainder of the species data is taken from several other sources, namely the thermodynamic tables of Gurvich *et al.* [55], the NIST Thermochemical Research Center (TRC) tables [56], and the NIST-JANAF thermochemical tables [57, 58]. The thermodynamic data in CEA is presented in the form of 7-coefficient polynomials for the specific heat of each species with an additional coefficient for computing the species enthalpy and entropy (for a total of 9 coefficients) as a function of temperature at the standard state pressure. While the CEA database is used extensively, several drawbacks may decrease the overall accuracy of computations made using its dataset. For example, the database has been constructed using a range of computational methods and experimental results, without regard to the consistency of species enthalpies of formation.

Ruscic *et al.* [59, 60] introduced the concept of the thermochemical network (TN) which relates the species enthalpy of formation to one another through thermochemically relevant data from literature. A TN can be used to develop a statistically correlated set of formation enthalpies across all of the species in the database. This ensures consistency in the formation enthalpy for each species and improves the estimated accuracy of each value. Furthermore, a TN allows new data to be processed easily and provides insight into which experimental or numerical investigations can most readily impact and expand the currently available set of thermochemical information. The Argonne National Laboratory (ANL) maintains an updated TN published in the Active Thermochemical Tables (ATcT) [61] which is considered the most accurate and self consistent source for species formation enthalpies. At the time of this article, the ATcT comprised of more than 560 species containing only C, H, O, and N.

While the ATcT provides a set of consistent formation enthalpies for many species, it does not provide the additional thermodynamic data required to build a useful database. However, Burcat *et al.* [62] currently maintain a vast thermodynamic database which is linked to the formation enthalpies provided by the ATcT. In total, it consists of 1031 species with the desired elements, of which, 249 have been linked to the ATcT. The majority of the species thermodynamic data in Burcat's database were selected from a range of sources

including CEA and journal articles. In addition, more than 300 species have been updated based on quantum mechanical calculations using the so called G3B3 methodology [62].

Blanquart *et al.* [63–66] have computed thermodynamic properties for large polycyclic aromatic hydrocarbons (PAH) for the study of soot formation. The database currently includes 64 PAH species ranging from benzene (C_6H_6) to coronenen ($C_{24}H_{12}$). Optimized geometric structures of each molecule were obtained using the B3LYP/6-31++G(d,p) method. Enthalpies of formation were determined using the G3MP2//B3 method with group corrections to account for systematic inaccuracies and are consistent with ATcT.

Finally, Goldsmith *et al.* [67] have recently computed highly accurate thermochemical data for 219 small hydrocarbon species using the RQCISD(T)/cc-PV∞QZ//B3LYP/6-331++G(d,bp) method to compute electronic energies. Consistency with the ATcT was also ensured by using a bond additivity correction method which removed systematic errors in the enthalpy of formation of each species.

3.2. Compilation Methodology

In order to compile a composite database from the sources discussed above, several steps were required.

3.2.1. Species Identification

The first step necessary to combine any data is to determine the exact chemical structure associated with each species in each data source. This includes a species' geometrical structure (chemical formula and isomerization) and electronic structure. In general, each thermodynamic database uses a variety of naming and documentation conventions to identify a particular species. For the databases considered in this work, the following conventions were used to represent the geometrical structure of individual species:

- CAS registry number: The Chemical Abstract Services (CAS) provides a unique numeric identifier for chemical substances.
- InChI and InChIKey: The International Chemical Identifier (InChI) provides a unique ASCII expression and its corresponding 27 character hash key (called InChIKey) to identify molecular structures.
- IUPAC name: The International Union of Pure and Applied Chemistry (IUPAC) provides a standardized naming convention for molecular structures.
- SMILES string: The simplified molecular-input line-entry system (SMILES) provides a line notation for representing geometrical structure of chemical species using ASCII text [68–70].

Several online search engines allow chemical structures to be searched using the above identifiers including NIST [71], PubChem [72], and the Chemical Identifier Resolver [73]. For species data containing one or more of these identifiers, the chemical structure was determined through one of the listed search engines, and a unique identifier was given to each separate chemical structure identified in all of the data sources. The remainder of the species for which no unique identification was given, the exact structure was determined by

Table 2: Hierarchy of thermodynamic databases based on consistency with the ATcT and accuracy of the data provided.

Rank	Database	No. of Species	Consistency with ATcT	References
1.	Goldsmith	219	Full	[67]
2.	Blanquart PAH data	64	Full	[63–66]
3.	Burcat	1031	Partial (249)	[62]
3.	CEA	193	None	[36, 50–52]

reviewing the original source of the thermodynamic data or inferred from other comments associated with the species in the database. In total, 1257 unique species (chemical structures) were identified out of the 1507 individual species records provided in the data sources used.

3.2.2. Hierarchy of Thermodynamic Data

A hierarchy of thermodynamic data was developed in order to choose which source of data to use for a species which was available in multiple databases. Namely, data sources were ranked first, based on their consistency with the ATcT enthalpies of formation and then second, based on the accuracy of the thermodynamic data provided. Based on these criteria, the data sources reviewed in the previous section are ranked in Table 2.

The Burcat and CEA databases are equally ranked because they are a conglomeration of several different data sources with no regard to self consistency. If a species was found in both Burcat and CEA (and not in a higher ranked database), then the data source with the most recent reference was typically chosen. However, a species in Burcat which was consistent with ATcT was always preferred over CEA regardless of the reference.

3.2.3. Treatment of Isomers, Conformers, and Electronic States

Isomers are a collection of species which share the same chemical formula (ie: same number of each constituent atoms) but have different chemical structures. Conformers (or conformational isomers) share the same chemical structure, but differ in the orientation around one or more bonds. The treatment of isomers varies between (and often within) thermodynamic databases. Nominally, all electronic states and conformers should be considered in the calculation of thermodynamic properties for a given isomer, and each isomer should be treated as a separate species. However, for some databases, isomers are grouped into a single species and the average thermodynamic properties are provided. In other cases, only a single isomer is considered. In this work, we have chosen to retain the highest level of information for isomers available for a particular chemical formula.

The same is true for electronic states of individual species. Treatment of electronic states typically falls into one of three categories.

1. Energy of excited states is very high compared to that of the ground state. These states will have a negligible contribution to species thermodynamic properties at lower temperatures and can be neglected. This is particularly true for large species which are expected to dissociate below the temperature at which the errors in neglecting excited states becomes important.
2. Excited electronic states are close in energy to the ground state but are expected to follow a Boltzmann distribution. In this case, the species thermodynamic properties may be treated as a Boltzmann-averaged ensemble of the ground and excited states.
3. Excited electronic states are close in energy to the ground state and cannot be assumed to be in equilibrium with the ground electronic state. These states are often treated as separate pseudo-species. For example, the singlet and triplet states of C_2 are often treated separately as they are known to be out of equilibrium with one another.

As was done with isomers, we have elected to retain all separate electronic states when available, in place of computing Boltzmann-averaged properties. Note however, that separating electronic states in this way has no effect on equilibrium species concentrations when all states are summed.

3.2.4. Excluded Species

Though thermodynamically viable, some species in the considered databases matching all of the above criteria were simply not kinetically viable based on the timescales of interest. In particular, all linear carbon molecules, C_n and C_nH for $n > 6$, and fullerenes such as C_{70}, were excluded from the final database.

The final database consists of 1257 unique species which have been selected from a total of 1768 entries in the databases discussed in the previous section. The majority of the species have been taken from the thermochemical tables of Burcat. 197 are taken from the work of Goldsmith and 64 others from Blanquart. The full database is provided in a text file as supplementary material to this article.

3.3. Comparison of Detailed Model with CEA

The new database has been evaluated by comparing equilibrium mixture properties to that of the CEA database. The mixtures were chosen to represent typical elemental compositions experienced during entry into Earth and Martian atmospheres. In particular, two such compositions are studied: (i) a mixture of 10 % CO_2 with 90 % pyrolysis gas by volume is used to represent the boundary layer of a Martian entry contaminated with pyrolysis gases, and (ii) a mixture of 10 % air and 90 % pyrolysis gas to simulate the same for Earth. The elemental composition for air is given in Table 1 and the pyrolysis gas composition was computed with Eqs. (12) and (13) assuming a pure phenol (C_6H_5OH) resin and a char yield of 50 %.

3.3.1. Equilibrium Compositions

Fig. 3 compares the major species mole fractions for the CO_2/pyrolysis mixture at 0.1 atm over a range of temperatures representative of a typical hypersonic boundary layer, computed using the detailed database

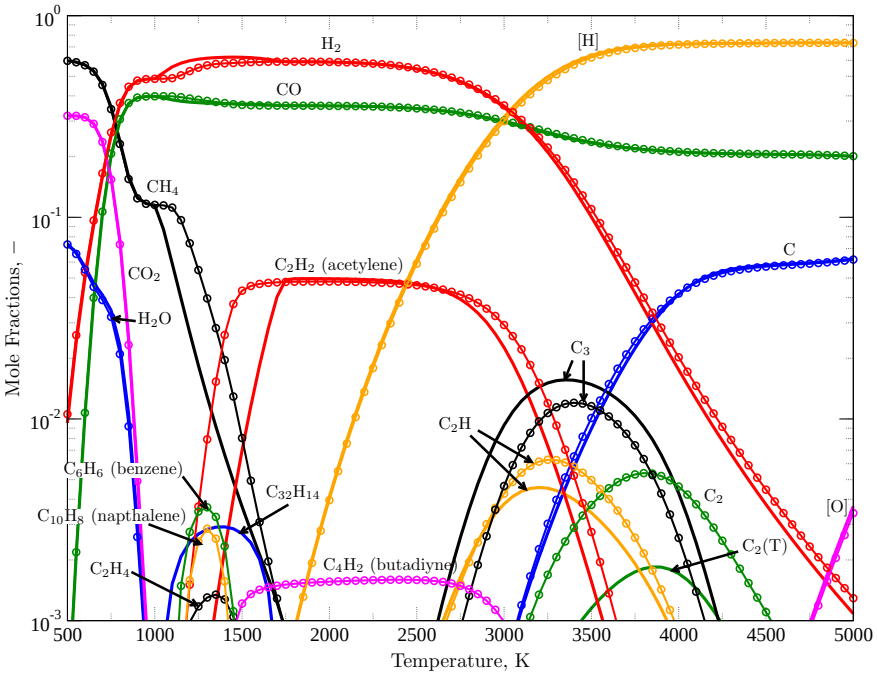

Figure 3: Comparison of the mixture equilibrium mole fractions computed with the detailed database (lines) and the CEA database (lines+symbols) for a 10 % CO_2 + 90 % pyrolysis gas mixture at a pressure of 0.1 atm. Square brackets around the species names indicate that the source of data in the detailed database is the CEA data.

constructed in this work and with the CEA database. The species whose thermodynamic data source were taken directly from CEA have been enclosed in square brackets in order to clearly distinguish which species have been updated. As can be seen in Fig. 3, there are two significant differences between the mole fractions computed using this database and CEA. The first occurs between 1000 K and 1800 K where the concentrations of CH_4 and C_2H_2 computed with the CEA model are much higher. The carbon contained in these molecules as well as C_2H_4, naphthalene, and benzene in the CEA solution have been replaced by one large PAH, $C_{32}H_{14}$, which is not present in the CEA database. This suggests that the solution is trying to maximize the number of C–C bonds present in the mixture which may indicate that the mixture is likely to produce condensed carbon (soot) at this temperature. This phenomena also provides a slight increase in the H_2 mole fraction in this temperature region as the number of C–H bonds decrease. The second significant difference occurs between about 2500 K and 4500 K. In this region, the new database predicts a higher C_3 concentration while the concentrations of C_2H and C_2 are reduced. Note that in the present work, both the singlet and triplet electronic states are included for C_2 whereas in the CEA database, only the equilibrium composition of C_2 is present.

Fig. 4 shows the major and minor equilibrium mole fractions for the 10 % air + 90 % pyrolysis gas mixture under the same conditions as before. From the figure, it is clear that similar observations may be made as

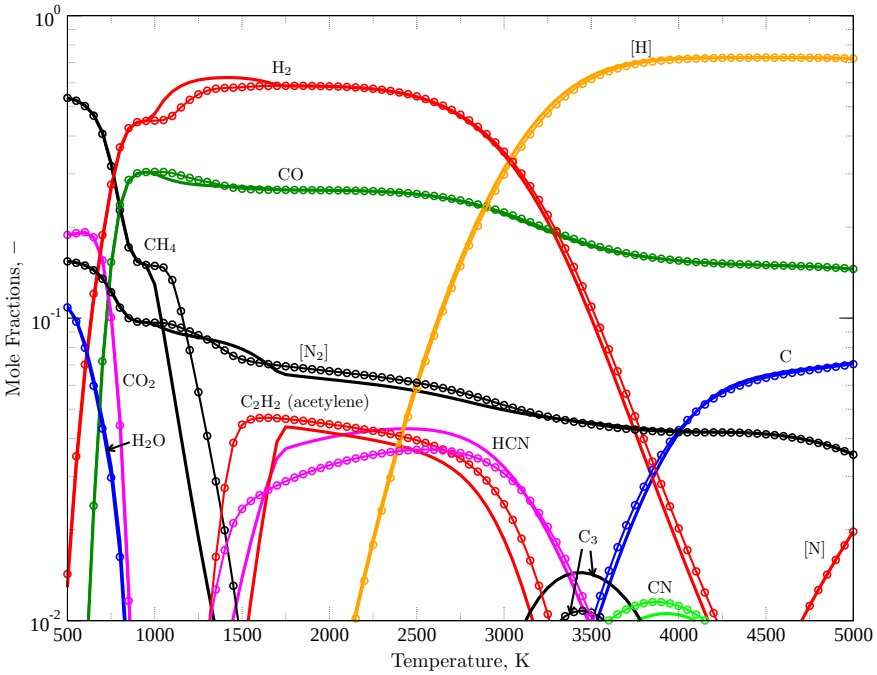

(a) Major species.

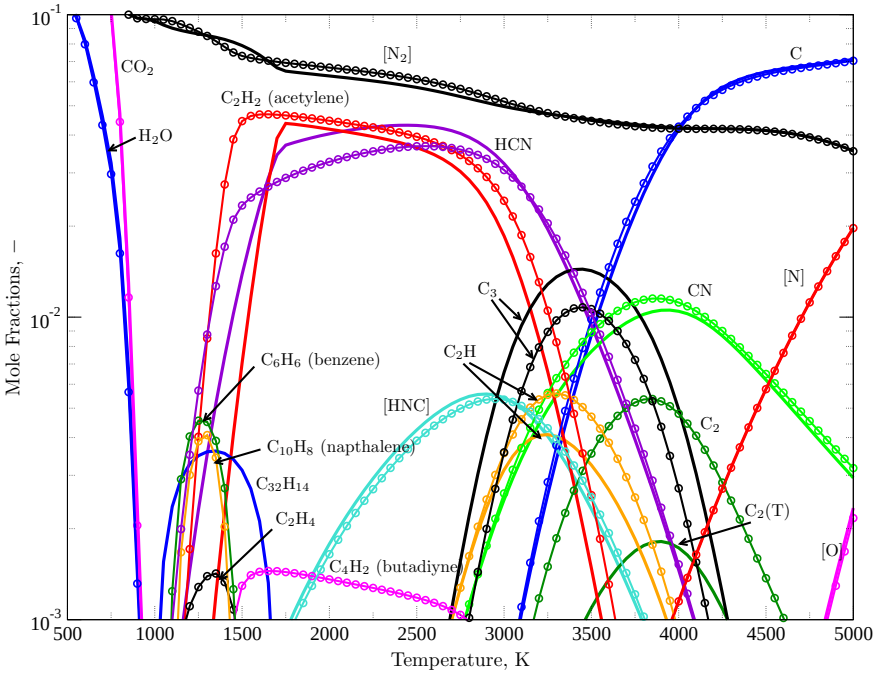

(b) Minor species. CH_4, H_2, CO, and H are not shown for clarity.

Figure 4: Comparison of the mixture equilibrium mole fractions computed with the detailed database (lines) and the CEA database (lines+symbols) for a 10 % air + 90 % pyrolysis gas mixture at a pressure of 0.1 atm. Square brackets around the species names indicate that the source of data in the detailed database is the CEA data.

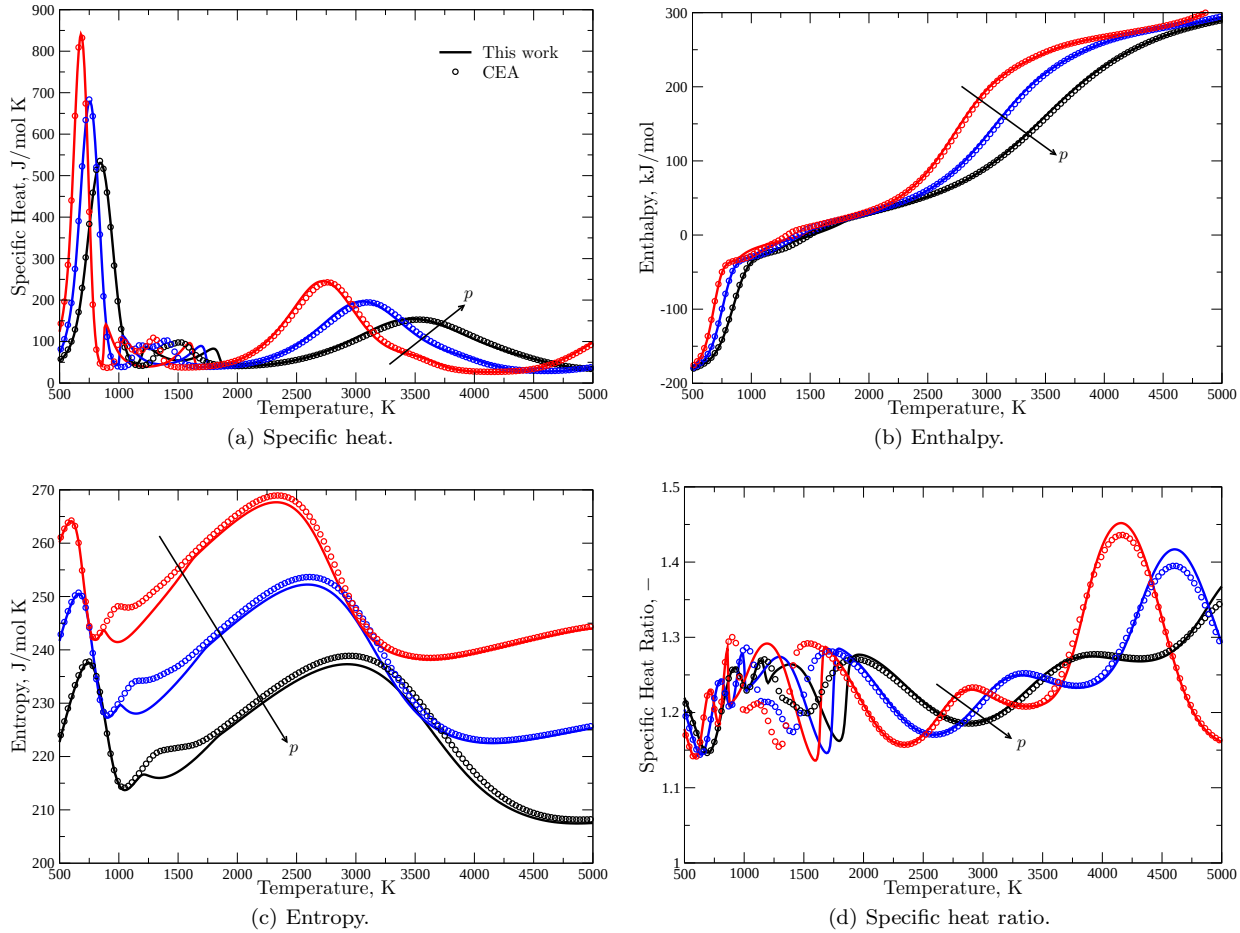

(a) Specific heat. (b) Enthalpy. (c) Entropy. (d) Specific heat ratio.

Figure 5: Comparison of the mixture equilibrium thermodynamic properties between the detailed database and CEA for an elemental composition of 10 % CO_2 + 90 % Pyrolysis Gas and pressures of 0.01 atm, 0.1 atm, and 1 atm. Arrow indicates increasing pressure.

were discussed for the CO_2/pyrolysis mixture.

3.3.2. Equilibrium Thermodynamic Functions

The differences in species mole fractions for the compositions studied in Figs. 3 and 4 have a substantial effect on the mixture thermodynamic properties as well. Fig. 5 compares the mixture specific heat at constant pressure, enthalpy, entropy, and specific heat ratios, at various temperatures and pressures, computed with the CEA database and the detailed model for the CO_2/pyrolysis mixture of Fig. 3. From the figures, the effect of the addition of $C_{32}H_{14}$ into the database is clearly seen in all the mixture thermodynamic properties at low temperatures. The oscillatory nature of the specific heat shown in Fig. 5a is due to the reactive c_p term from Eq. 7. The peaks in c_p correspond to the peaks in the mole fraction gradients at those temperatures and are thus related to the balance between global reactions taking place as the temperature is increased. From Fig. 5b, the equilibrium mixture enthalpy is not significantly affected by the improvement

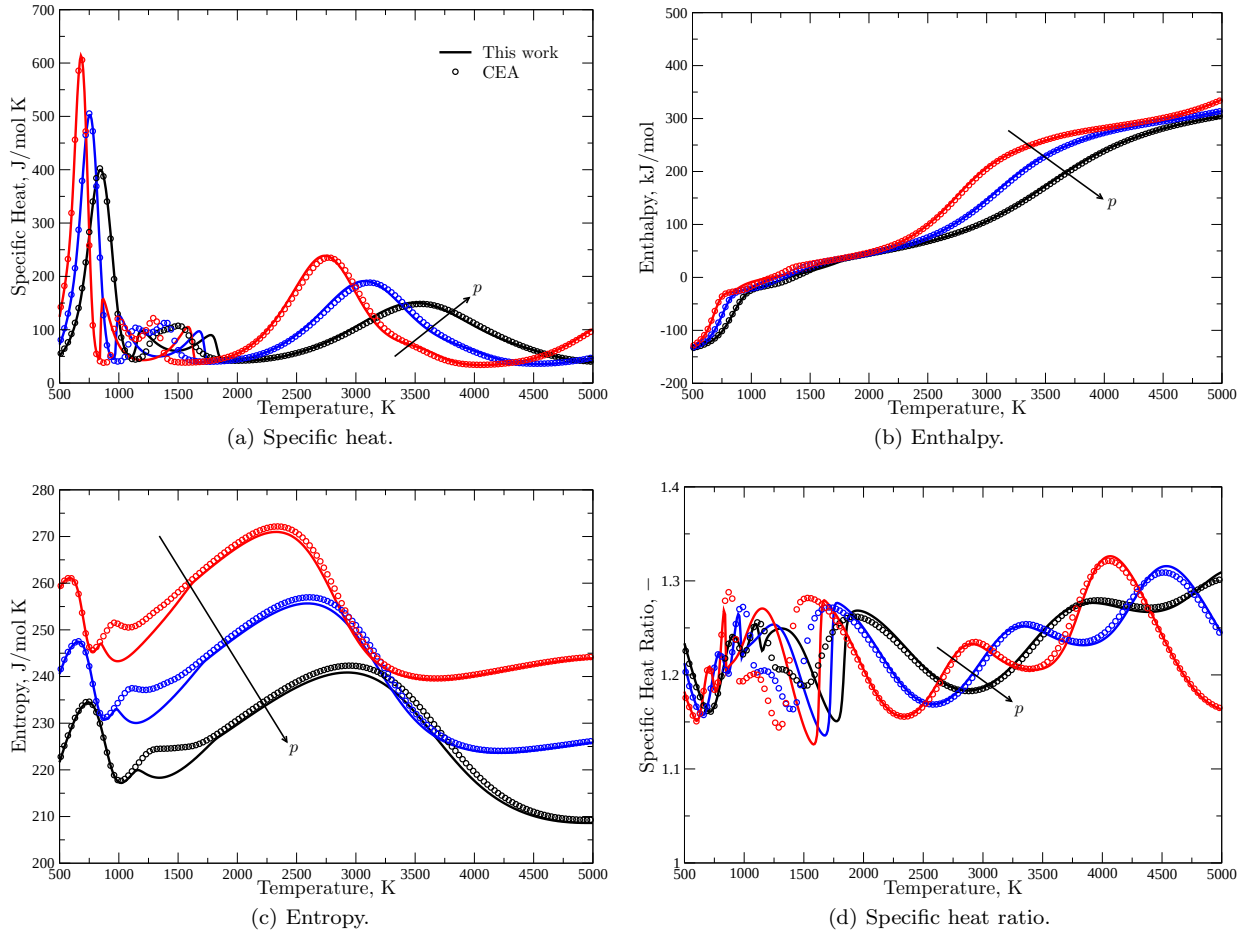

(a) Specific heat.

(b) Enthalpy.

(c) Entropy.

(d) Specific heat ratio.

Figure 6: Comparison of the mixture equilibrium thermodynamic properties between the detailed database and the CEA database for an elemental composition of 10 % air + 90 % Pyrolysis Gas and pressures of 0.01 atm, 0.1 atm, and 1 atm. Arrow indicates increasing pressure.

in the thermodynamic database.

A similar comparison is also made for the mixture thermodynamic properties of the air/pyrolysis mixture in Fig. 6 corresponding to the same conditions as in Fig. 5.

3.3.3. Equilibrium Surface Ablation Rates

If one considers a thin control volume over the surface of an ablating thermal protection system and assumes that the flow through this volume is steady with equal diffusion coefficients for each species, then conservation of elements inside the control volume yields

$$y^e_{w,k} = \frac{B'_c\, y^e_{c,k} + B'_g\, y^e_{g,k} + y^e_{e,k}}{B'_c + B'_g + 1} \quad \forall\, k \in \mathcal{E}, \tag{15}$$

where the subscripts w, c, g, and e refer to wall, char, pyrolysis gas, and boundary layer edge properties respectively, and $B' \equiv \dot{m}/(\rho_e u_e C_M)$, with C_M the local Stanton number for mass transfer, represents a

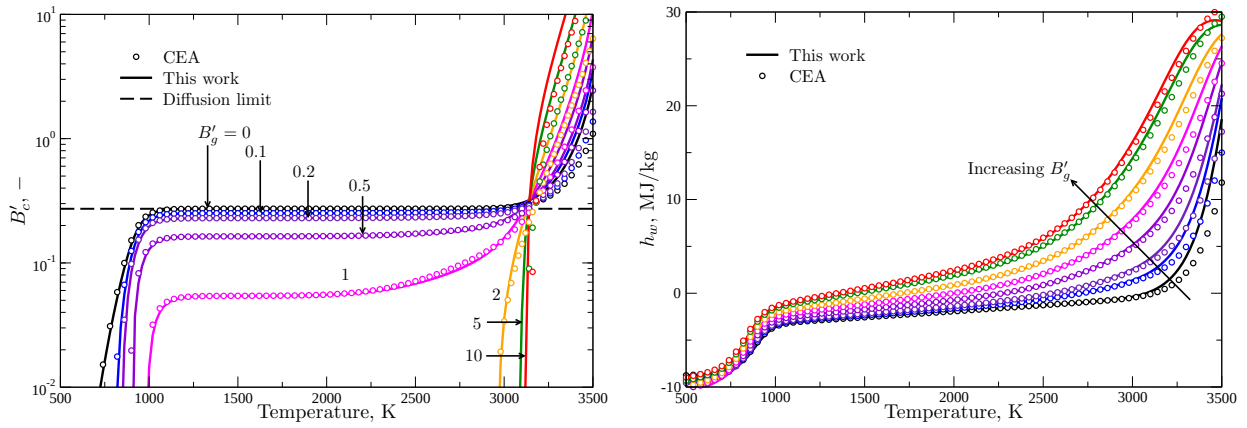

(a) Char blowing rate. (b) Wall enthalpy.

Figure 7: Comparison of equilibrium char blowing rates and wall enthalpies for a pure graphite surface in a CO_2 atmosphere at 0.1 atm computed with the detailed database and CEA. The theoretical diffusion limited blowing rate corresponds to a pyrolysis gas mass flux of zero.

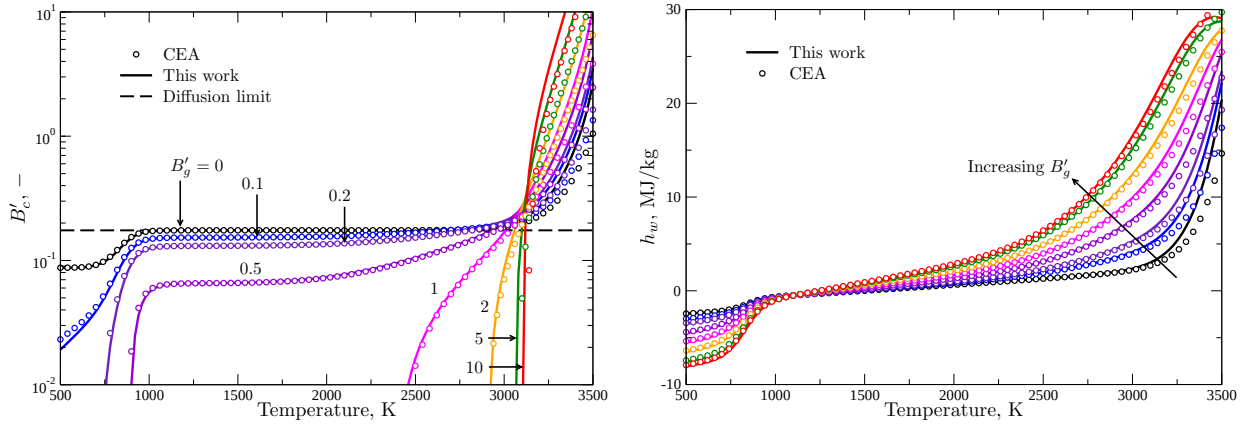

(a) Char blowing rate. (b) Wall enthalpy.

Figure 8: Comparison of equilibrium char blowing rates and wall enthalpies for a pure graphite surface in air at 0.1 atm computed with the detailed database and CEA. The theoretical diffusion limited blowing rate corresponds to a pyrolysis gas mass flux of zero.

mass flux nondimensionalized by the boundary layer edge mass flux. Reference [25] provides more details regarding this control volume analysis. Assume that the gas in the thin control volume is in equilibrium with the surface of the ablator, Eq. 15 may be solved simultaneously with the minimization of the mixture Gibbs free energy at a fixed T, p, and B'_g, and known boundary layer, pyrolysis gas, and char, elemental compositions, to compute the elemental mass fractions at the surface of the ablator $y^e_{w,k}$ along with the non dimensional ablation rate B'_c. In this section, several such computations have been performed to assess the possible effects of the updated thermodynamic data on surface recession and wall enthalpies as compared to those computed with the CEA data.

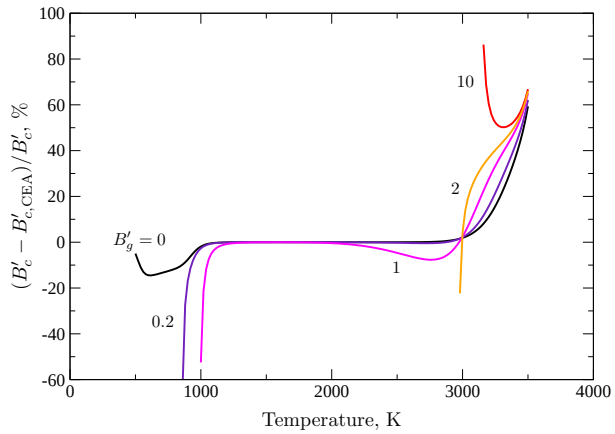

Figure 9: Differences in the computed B'_c curves shown in Fig. 7 curves resulting from the detailed database and CEA for select values of B'_g

Figs. 7 and 8 present the equilibrium char blowing rates and wall enthalpies for a graphite char in both CO_2 and air at 0.1 atm with varying pyrolysis gas blowing rates. The composition of the pyrolysis gas is taken to be the same as was used in the previous comparisons for the sake of simplicity. Char blowing rates are typically characterized by three distinct regions: i) the reaction limited regime, ii) the diffusion limited regime, and iii) the sublimation regime. The reaction limited regime occurs at low temperatures in which the rate of surface removal reactions, such as oxidation of the surface, are limited by the available energy at the surface for promoting the reactions. As the temperature increases, these processes become limited by the amount of gas phase reactants reaching the surface through diffusion. Finally, when the temperature is high enough, the surface begins to sublimate and no longer requires reactants present at the surface. Under the assumption of equilibrium, surface removal cannot be limited by reactions. However, the diffusion and sublimation regimes are clearly present in Figs. 7 and 8. The plateaus visible in the middle temperature range of both figures correspond to the maximum formation of carbon monoxide by surface oxidation. As the pyrolysis mass flux increases, the available oxygen at the surface decreases causing this plateau to shift down. A second plateau is seen in Fig. 8 below about 750 K for $B'_g = 0$ due to the stable formation of carbon dioxide. Finally, sublimation dominates above 3000 K.

Fig. 9 shows the relative difference in the computed B'_c curves of Fig. 7. The surface recession rate of an ablating heat shield is simply the mass flux of the ablating char layer divided by the char density,

$$\dot{s}_c = \frac{\dot{m}_c}{\rho_c} = \frac{\rho_e u_e C_M}{\rho_c} B'_c. \tag{16}$$

Thus, the percent difference between the B'_c values shown in Fig. 9 loosely correspond to the difference in surface recession rates that would be predicted by a material response model using the database presented here and the CEA database, for an isothermal surface. As a concrete example, for the conditions in Fig. 7, with a fixed surface temperature of 3200 K and pyrolysis gas blowing rate equal to the rate of boundary

layer gases diffusing to the surface ($B'_g = 1$), the update in the thermodynamic data corresponds to a 38 % increase in the surface recession rate as predicted using the CEA database. It should of course be noted however, that such differences will be lessened when a full surface energy balance is accounted for. In that situation, the temperature is likely to decrease slightly to account for the increased blowing rate and thus make the differences in blowing rate negligible.

4. Development of Reduced Models

The full database presented in the previous section provides an extensive list of more than 1200 species which may be formed at equilibrium for a wide range of conditions. In practice, many species in the detailed list have equilibrium concentrations which provide a negligible contribution to mixture thermodynamic properties. In general, the computational effort to compute a single equilibrium composition is small, even when including more than 1200 species. However, the use of equilibrium models in conjunction with CFD to model the response of thermal protection systems subjected to high-enthalpy flows may require tens of thousands of these calculations during the iteration process which can quickly dominate the CPU cost of the simulation when many species are considered. For mixtures with constant elemental compositions, tables of precomputed properties versus temperature and pressure can be used to virtually eliminate this cost. However, this is rarely the case for carbon-phenolic mixtures due the mixing of pyrolysis, ablation, and atmospheric gases, as shown in Sec. 2.2.3.

The goal of the reduction procedure detailed in the following sections is to provide a reduced set of species out of the full set which provide accurate equilibrium mixture thermodynamic properties over the temperature, pressure, and composition range of interest. Beyond improving the CPU costs of computing equilibrium properties, the reduced species sets also highlight the most important species and can serve as a guide for future thermodynamic database improvements as well as a starting point for developing finite-rate chemistry mechanisms for carbon-phenolic mixtures.

4.1. Reduction Methodology

Previous model reduction studies for carbon-phenolic ablation in air have used either mole fraction tolerances for simulated pyrolysis gas flows in or out of equilibrium [30, 74, 75] or tolerances on computed B'_c values [76] to trim species from the detailed model. Typically, these reduced sets are only valid for a limited number of conditions which were used in the reduction process, and usually incorporate additional species based on the authors' best judgment to account for specific reaction dynamics or import radiators. Such approaches do not take into consideration the mixture thermodynamic properties of the reduced sets, and therefore risk inaccurate predictions of mixture bulk properties. In addition, it is difficult to extend these approaches to other gases or conditions of interest such as atmospheres rich in CO_2. In the following, a consistent method is proposed which ensures mixture thermodynamic properties are accurately reproduced

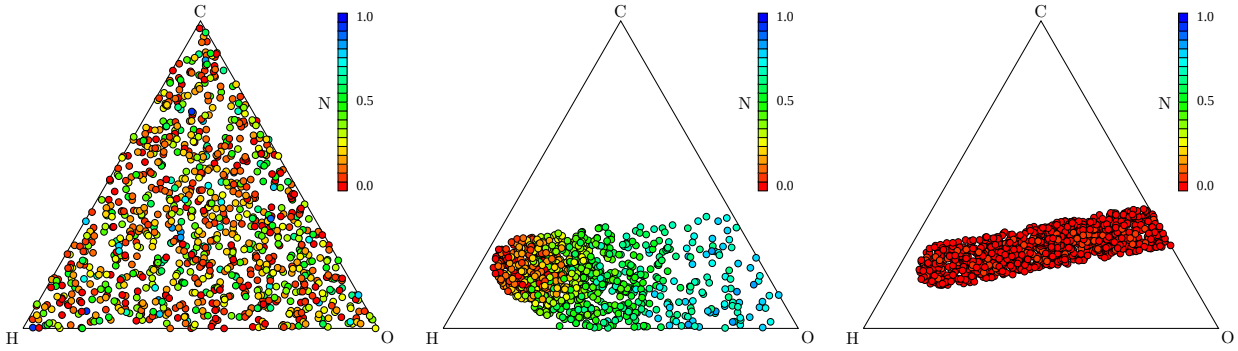

(a) $\mathcal{R}_1$: Unit simplex. (b) $\mathcal{R}_2$: Mix of air and pyrolysis gas. (c) $\mathcal{R}_3$: Mix of CO_2 and pyrolysis gas.

Figure 10: Discrete elemental composition spaces (projected onto the C-H-O simplex) used to generate the reduced models. Color represents nitrogen mole fraction.

by the reduced model over all conditions of interest. The method is then applied to generate reduced species sets for all the elemental composition, temperature, and pressure spaces of interest.

4.1.1. Reduction Spaces

A reduction space, denoted $\mathcal{R}$, is first defined as the region of interest in the temperature, pressure, and composition space for which a reduced species set should be determined. In general, all reduction spaces are subsets of the following space:

$$\mathcal{R} = \left\{ P = (T, p, x^e) \ : \ T, p, x_k^e \in \mathbb{R}^+ \ \forall \ k \in \mathcal{E} \quad \text{and} \quad \sum_{k \in \mathcal{E}} x_k^e = 1 \right\}. \tag{17}$$

In other words, temperatures, pressures, and mole fractions must be non-negative with elemental mole fractions summing to unity. Note for a given point, P, all equilibrium thermodynamic functions are completely defined.

Three discrete reduction spaces are considered in this work, though the proposed methodology could be extended to other spaces as well. Each reduction space uses the same temperature and pressure distribution consisting of 50 temperatures ranging linearly from 500 K to 5000 K and 10 pressures varying logarithmically from 0.001 bar to 10 bar. Three different compositions spaces, consisting of 1000 composition points, were used to form the three reduction spaces. Each reduction space then consists of every combination of temperature, pressure, and composition, for a total of 500 000 discrete points each.

Fig. 10 provides the three sets of elemental compositions used in this work for generating the reduction spaces. The first set in Fig. 10a, represents a uniform distribution over the entire C-H-O-N simplex, which is the most general composition space. The other two composition spaces limit the compositions considered to mixtures of air (Fig. 10b) or CO_2 (Fig. 10c) and pyrolysis gas. These were generated by creating a uniform distribution of points inside the hypercylinder which connects the atmosphere and pyrolysis gas compositions. The diameter of these cylinders was taken to be 10 % of the Euclidean distance between the

two compositions to allow for perturbations due to diffusion to be taken into account in the reductions.

4.1.2. The Thermodynamic Error Function

Denoting any mixture averaged thermodynamic function, f, computed with a species set, $\mathcal{S}_s$, at a temperature, pressure, and composition point, P, as $f^s(P)$, the maximum error in f using a species subset, $\mathcal{S}_s$, over the entire reduction space, $\mathcal{R}_r$, is given by

$$\tilde{f}_{rs} = \max_{P \in \mathcal{R}_r} \left| \frac{f(P) - f^s(P)}{f(P)} \right|. \tag{18}$$

We now define a thermodynamic error function for a reduction space $\mathcal{R}_r$ and species set $\mathcal{S}_s$, denoted Θ_{rs}, which corresponds to the maximum error in c_p, $\delta h \equiv h(T) - h(T^\circ)$, and s over the given reduction space as compared to the full set of species.

$$\Theta_{rs} = \max_{f \in \{c_p, \delta h, s\}} \tilde{f}_{rs}. \tag{19}$$

The difference $h(T) - h(T^\circ)$ is used instead of $h(T)$ in order to prevent the denominator of Eq. 18 from being close to zero at low temperatures and because δh is strictly positive.

It now suffices to say that the goal of the reduction procedure, for a given reduction space, is to find the smallest species subset whose thermodynamic error function satisfies a given tolerance, τ.

$$\mathcal{S}_r^{\text{red}}(\tau) = \underset{\{\mathcal{S}_s \,:\, \Theta_{rs} \leq \tau\}}{\arg\min} |\mathcal{S}_s| \tag{20}$$

In principle, this is a simple task as it is possible to directly compute Θ_{rs} given a species set $\mathcal{S}_s$. All that is required is to enumerate all possible combinations of species from the full set, for increasing subset sizes, until a set that satisfies Eq. 20 is reached. In practice however, this is a highly intractable problem with the computer power available today. For example, consider that there are over 10^{20} possible species combinations of 20 species from a set of 100. Therefore, an alternate procedure which attempts to find reduced sets in a reasonable CPU time is described in the next section. Although the reduced sets are not guaranteed to be "optimal" in terms of their size with respect to their accuracy, it will be shown that they are small enough to be used in most applications.

4.1.3. Reduction Procedure

To begin, the assumption is made that there exists an ordered set of species such that the subset created by adding each successive species in the list generates a smaller thermodynamic error function than the previous subset, ie:

$$\mathcal{A} = \{A_j \;:\; \Theta_{r,j} > \Theta_{r,j+1} \quad \forall\, j \in \mathcal{S}\}, \tag{21}$$

where A_j represents the j^{th} species in the list and the subscript j in $\Theta_{r,j}$ refers to the species subset generated by combining species 1 to j in the list $\mathcal{A}$. Intuitively, this is not a bad assumption, because in general, adding species to a subset should improve the overall accuracy. The goal is then to find such an

ordered list which minimizes $\Theta_{r,j}$ for each j. This is a far simpler problem then determining the optimum reduction as described in the previous section because it requires a small number of species combinations to evaluate by comparison.

The first step in the procedure requires generating an initial guess of the "optimum" species order. This is done by first considering the error function for the mixture enthalpy shifted by the enthalpy at the standard state temperature. Inserting Eq. 4 in Eq. 18 provides

$$\widetilde{\delta h}_{rs} = \max_{P \in \mathcal{R}_r} \left(\frac{1}{\delta h} \left| \sum_{j \in \mathcal{S}_s} (y_j - y_j^s) \delta h_j + \sum_{j \in \mathcal{S} - \mathcal{S}_s} y_j \, \delta h_j \right| \right). \tag{22}$$

From the above, it is clear that there are two components of error introduced by a reduction in the species set. The first comes from the difference in the equilibrium composition obtained with the reduced set as compared to the full set. The second is due to the enthalpy contribution of the species which are not included in the reduced model in the overall mixture enthalpy. Interestingly, this component of the error can be computed *a priori* without need of computing equilibrium compositions of the reduced set. In addition, it is clear that this error contribution will grow monotonically as species are removed from the full set because it is a sum of only positive values. Based on these facts, the initial ordering is determined such that the maximum enthalpy contribution of each species is strictly decreasing, or

$$\max_{P \in \mathcal{R}_r} \left| \frac{y_j \, \delta h_j}{\delta h} \right| > \max_{P \in \mathcal{R}_r} \left| \frac{y_{j+1} \, \delta h_{j+1}}{\delta h} \right|, \quad \forall \, j \in \mathcal{S}.$$

After an initial species order is determined, $\Theta_{r,j}$ is computed for each index j. It is useful to note that, once it is computed, swapping species A_j with A_{j+1} only affects the error function at index j. This comes from the fact that the ordering only applies to species which are included in the species subset for a given index, however, the ordering within a particular subset has no effect on the equilibrium properties of the mixture. Based on this simple fact, an algorithm has been developed to improve a given species ordering to minimize $\Theta_{r,j}$ for each index j. Forward and reverse improvement sweeps are performed by looping over the species index j and checking if swapping the species j and $j+1$ lowers $\Theta_{r,j}$. If it does, the ordering is updated, otherwise the loop simply continues.

Fig. 11 shows the result of this reduction procedure for the reduction space $\mathcal{R}_2$. For this case, 7 forward and reverse sweeps were required to reach the final ordering. The general trend in the thermodynamic error function for the final ordering suggests that the equilibrium thermodynamic properties of the mixture are highly sensitive to relatively few species. As each of these species are added to the reduced set, the error drops quickly. However as more species are added, the corresponding improvement in the error function decreases until adding new species provides little benefit. This is clearly demonstrated in Fig. 11a which shows that in order to improve the error function from 10 % to 5 %, only 3 additional species are required, while dropping from 5 % to 1 % requires 13.

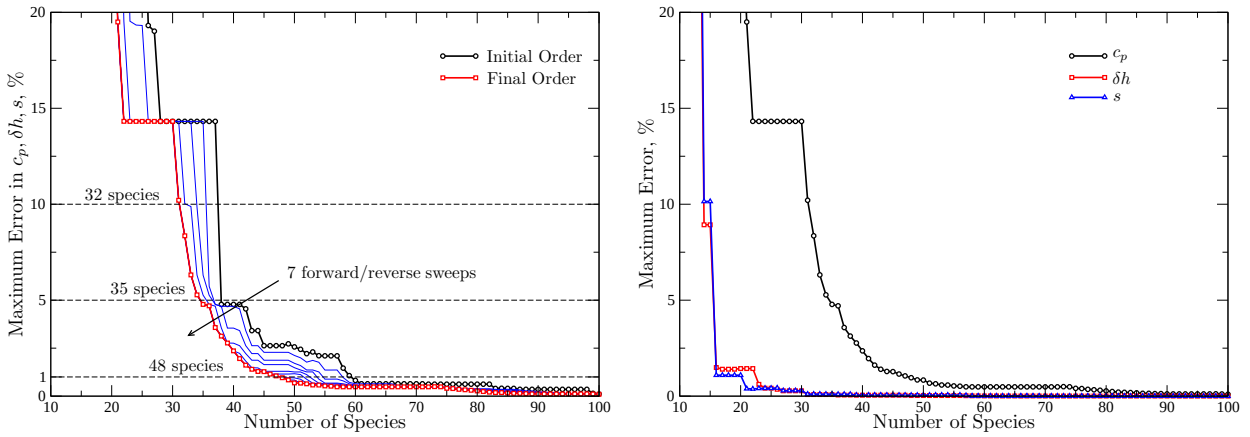

(a) Reduction history. Seven forward and reverse sweeps were required before the optimum ordering was reached.

(b) Maximum errors in thermodynamic properties for final reduction.

Figure 11: Thermodynamic error function versus number of included species for the $\mathcal{R}_2$ reduction space.

Fig. 11b shows the maximum error in each thermodynamic property for the reduced species set corresponding to the $\mathcal{R}_2$ reduction space. It is clear from the figure that the error in c_p is the dominant contribution to the thermodynamic error function. Inserting Eq. 7 into Eq. 18, we have

$$\widetilde{c_p}_{rs} = \max_{P \in \mathcal{R}_r} \left[\frac{1}{c_p} \left| \sum_{j \in \mathcal{S}_s} (y_j - y_j^s) c_{p,j} + \left(\frac{\partial y_j}{\partial T} - \frac{\partial y_j^s}{\partial T}\right) h_j + \sum_{j \in \mathcal{S} - \mathcal{S}_s} y_j \, c_{p,j} + \frac{\partial y_j}{\partial T} h_j \right| \right], \tag{23}$$

which indicates that the error in the specific heat depends on the partial derivative of the species mass fraction with temperature. Using Figs. 3 and 4 comparing species mole fractions computed with the full database and the much smaller CEA database as examples, the species mass fraction gradients can vary significantly over temperature, and are particularly sensitive to the included species in the database. Therefore, it is the reactive c_p which contributes most to the thermodynamic error function. This suggests that if the equilibrium mixture c_p is not required, it could be removed from the evaluation of Eq. 19 to produce significantly smaller reduced species sets.

4.2. Reduced Species Sets

For each of the reduction spaces described in the previous section ($\mathcal{R}_1$, $\mathcal{R}_2$, and $\mathcal{R}_3$), tolerances on the maximum thermodynamic error of 10 %, 5 %, and 1 % were used to create a total of 9 different reduced sets. We will denote a reduced set by $\mathcal{R}_r$-τ, for the reduction space r and error tolerance τ. For example, $\mathcal{R}_2$-5 indicates the reduced species set for the reduction space $\mathcal{R}_2$ and tolerance of 5 %. The number of species required for each reduced model is given in Table 3. The largest reduced set ($\mathcal{R}_1$-1), with 65 species, represents a reduction of nearly 20 times as compared to the full model which translates into large reductions in the computational costs associated with computing equilibrium compositions and mixture

Table 3: Summary of reduced species set sizes.

Reduction Space	Error Tolerance		
	10 %	5 %	1 %
$\mathcal{R}_1$: all compositions	49	54	65
$\mathcal{R}_2$: air / pyrolysis mix	32	35	48
$\mathcal{R}_3$: CO_2 / pyrolysis mix	23	24	35

thermodynamic properties. In particular, consider the solution of the equilibrium problem using the Gibbs function continuation method, as described in [38]. The dominant cost of this method is the singular value decomposition (SVD) of a matrix with m rows equal to the number of species and n columns equal to the number of elements considered in the mixture. The cost of an SVD is proportional to $O(m^2n + n^2m + n^3)$. Since, in practice, the number of species greatly outweighs the number of elements in a mixture, this cost can be treated as $O(m^2n)$. Therefore, a reduction in the number of species by 20 times, results in an approximately 400-fold decrease in the time required to compute the equilibrium concentrations.

Table 4 provides a list of the 66 species belonging to at least one reduced model. The notation from Frenklach *et al.* [77] has been used to represent all PAH's. In this notation, A_n denotes n aromatic rings and $(Ra)_n$ indicates n rings of a carbons each. Fig. 12 provides a few examples to clarify the notation. All PAH's are fully saturated unless explicitly written otherwise.

For each species, Table 4 lists the maximum tolerance level at which the species is included in each reduction space. For example, HCN is included in both the $\mathcal{R}_1$-10 and $\mathcal{R}_2$-10 sets, and is therefore also included in $\mathcal{R}_1$-5, $\mathcal{R}_1$-1, $\mathcal{R}_2$-5, and $\mathcal{R}_2$-1. Thus, each reduced species set may be enumerated based on Table 4. Interestingly, $CH(X^2\Pi)$ is required in $\mathcal{R}_2$-10 and $\mathcal{R}_3$-10 but does not belong to $\mathcal{R}_1$-10. This indicates that the larger composition space of $\mathcal{R}_1$ required another (or several other) species to reach a particular tolerance level which offset the error caused by not including $CH(X^2\Pi)$.

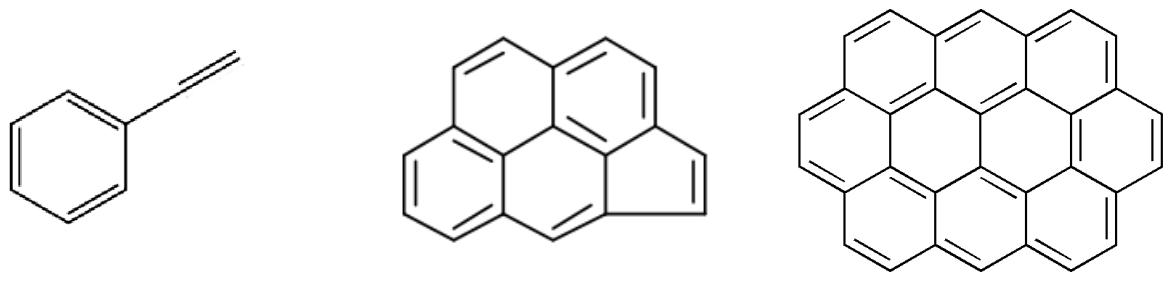

(a) Ethynylbenzene (A_1CH_2) (b) Cyclopenta[cd]pyrene ($A_4R\,5$) (c) Ovalene (A_{10})

Figure 12: Example PAH's.

Table 4: Summary of species belonging to the reduced mechanisms. Enthalpies of formation have been evaluated using the polynomial information data by each reference at 298.15 K.

No.	Species	Tolerance, %			Δh_f°	Ref.	No.	Species	Tolerance, %			Δh_f°	Ref.
		$\mathcal{R}_1$	$\mathcal{R}_2$	$\mathcal{R}_3$	kJ/mol				$\mathcal{R}_1$	$\mathcal{R}_2$	$\mathcal{R}_3$	kJ/mol	
1.	C	10	10	10	716.7	[36]	34.	C_4H_3	1	5	1	501.8	[62]
2.	C^+	10	10	10	1809.4	[36]	35.	CH_2CHCCH	5	1	1	289.1	[67]
3.	$CH(X^2\Pi)$		10	10	596.1	[67]	36.	CH_2CCCH_2	1			321.3	[67]
4.	HNC	10	10		194.4	[36]	37.	C_4N_2	10			529.2	[36]
5.	HCN	10	10		129.3	[64]	38.	C_5	10			1072.3	[64]
6.	CH_4	10	10	10	−73.9	[67]	39.	C_5H	10			932.2	[64]
7.	CN	10	10		438.7	[62]	40.	C_6H_2	10	10	10	700.8	[64]
8.	CO	10	10	10	−110.3	[67]	41.	C_8H_2	10	10	5	900.0	[62]
9.	CO_2	10	10	10	−394.2	[67]	42.	A_1C_2H	1	1	1	306.6	[64]
10.	$C_2(T)$	10	10	10	835.2	[67]	43.	C_9H_8	10	10	10	65.8	[62]
11.	$C_2(S)$	10	10	10	827.5	[67]	44.	$C_{10}H_2$	10	1		1120.0	[62]
12.	C_2H	10	10	10	568.1	[62]	45.	$HC_{11}N$	10			1270.0	[62]
13.	C_2H_2	10	10	10	228.9	[67]	46.	$C_{11}N$	10			1500.0	[62]
14.	$H_2CC(S)$	10		1	412.2	[67]	47.	$C_{12}H_2$	10			1340.0	[62]
15.	CH_3CN	1	1		74.0	[62]	48.	$A_4R\,5$	1			334.4	[64]
16.	C_2H_4	10	5	10	52.3	[67]	49.	$A_8(R\,5)4$	10			1139.3	[62]
17.	CNC	10			675.8	[62]	50.	$\cdot A_{10}$	10			663.5	[62]
18.	CCN	10			679.1	[62]	51.	A_{10}	10	10	10	418.4	[62]
19.	NCCN	10	1		309.1	[36]	52.	H	10	10	10	218.0	[36]
20.	:CNCN	10	10		413.0	[62]	53.	H^+	5			1536.2	[36]
21.	C_3	10	10	10	823.6	[62]	54.	OH	10	10	10	37.3	[67]
22.	C_3H	10	10		716.7	[64]	55.	H_2	10	10	10	0.0	[67]
23.	C_3HN	10	10		368.4	[62]	56.	H_2O	10	10	10	−243	[67]
24.	HCCCH(T)	10	1	1	546.8	[67]	57.	NH_3	10	1		−45.6	[62]
25.	$\cdot CH_2CCH$	5	5	1	351.5	[62]	58.	N	10	10		472.7	[36]
26.	$CH_2C\dot{C}H$	1	1	1	348.4	[62]	59.	NO	10	10		91.3	[36]
27.	CH_3CCH	1	1	1	185.5	[67]	60.	N_2	10	10		0.0	[36]
28.	CH_2CCH_2	1	1	1	188.8	[64]	61.	O(S)	5	1	1	438.5	[62]
29.	C_3O_2	5			−95.6	[62]	62.	O	10	10	10	249.2	[36]
30.	$C_4(S)$	10			1055.7	[62]	63.	O^+	1			1568.8	[36]
31.	$C_4(T)$	10			1059.7	[62]	64.	$O_2(S)$	1	1	1	94.4	[62]
32.	HCCCCH	10	10	10	460.2	[67]	65.	O_2	10	10	10	0.0	[67]
33.	CH_2CCCH	1	1		497.4	[67]	66.	e^-	10	10	10	0.0	[36]

5. Discussion

5.1. Contributions of PAH's

Figs. 3 through 6 show a significant deviation from equilibrium properties computed in CEA with the addition of the $C_{32}H_{14}$ (A_{10}, see Fig. 12) molecule to the database. In addition, other large polycyclic aromatic hydrocarbons (PAH) are present in the reduced species sets presented in Table 4 when the entire elemental composition space is considered. Large PAH's such as $C_{32}H_{14}$ are known to form during the combustion of lighter fuels like benzene or toluene, and act as precursors to the formation of soot particles which evolve over the course of combustion processes [64, 78]. For equilibrium calculations using highly carbon-rich mixtures, PAH's result from the maximization of the carbon to hydrogen atom ratio. However, while the creation of PAH's is thermodynamically feasible, it may not be kinetically viable in a real world

situation due to necessary residence times required for their creation. Rabinovitch [43] has studied this problem specifically for carbon-phenolic ablation and has shown that, up to the limit of available kinetic PAH data ($C_{18}H_{10}$), PAH's can form in significant quantities from the evolution of pyrolysis gases over typical residence times necessary for these gases to flow through a TPM. For this reason, these species have been retained in the detailed model presented in the previous sections.

5.2. Errors found during this work

Finally, it is worth noting a handful of errors found in the various data sources used during this work. As many species were found in multiple sources, this work provided an excellent opportunity to verify the data in each source through comparison with other sources. In some cases, discrepancies between two or more sources lead to the discovery of the following errors. These errors are enumerated below, as they may be helpful to other researchers, though the authors do not claim that other errors are not still present.

- *C_4 and C_5 from CEA* [36]: After comparison with calculations made by the authors, a significant discrepancy was found between C_4 and C_5 thermodynamic data and expected results. A careful review of the underlying data sources for these species revealed that the molecules' moment of inertia had been used in place of their characteristic rotational temperatures in the evaluation of thermodynamic properties.
- *NO^- from Burcat* [62]: The properties for NO^- have been updated after an error was found in the polynomial coefficients for c_p.

6. Concluding Remarks

This work developed a strategy for merging thermodynamic data sets based on their consistency with ATcT formation enthalpies and their estimated relative accuracy for use in carbon-phenolic ablation and pyrolysis simulation. In particular, over 1200 chemical structures comprised of C, H, N, and O were identified in four widely used thermodynamic databases.

Comparisons of computed equilibrium mole fractions and mixture thermodynamic properties between the detailed model and CEA showed some significant differences which could suggest errors in predicted heat loads on entry vehicles when using CEA thermodynamic data. In particular, the mixture specific heats and entropy were found to be sensitive to differences in the computed equilibrium mole fractions. Non-dimensional char blowing rates were also found to be sensitive to the thermodynamic data varying up to 80 % when using CEA compared to the database presented in this work.

In addition to the detailed database, a fast reduction methodology based on mixture equilibrium thermodynamic properties was developed. This procedure ensures the validity of mixture thermodynamic properties over the selected reduction space. Reductions were computed for several elemental composition, temperature, and pressure spaces related to typical problems encountered in the design of planetary entry vehicles.

It was found that only 32 and 23 species were required to model carbon-phenolic pyrolysis gas mixed with air and CO_2, respectively with reasonable accuracy.

Acknowledgments

J.B.S., B.B.F., and T.E.M. were funded by the European Research Council Starting Grant #259354: "*Multiphysics models and simulations for reacting and plasma flows applied to the space exploration program.*" A.M. was supported through NASA Award NNX13AN04A. J. L. was funded by the NASA Space Technology Research Grants Program, grant NNX12AG47A. J.R. and G.B. were funded by the U.S. Air Force Office of Scientific Research, grant FA9550-12-1-0472. Finally, the authors wish to thank Prof. Burcat for his timely and helpful answers to our questions.

[1] H. K. Tran, Development of Light Weight Ceramic Ablators and Arc-Jet Test Results, Tech. Rep. TM-108798, NASA, 1994.
[2] H. K. Tran, C. E. Johnson, D. J. Rasky, F. C. L. Hui, M.-T. Hsu, T. Chen, Y. K. Chen, D. Paragas, L. Kobayashi, Phenolic Impregnated Carbon Ablators (PICA) as Thermal Protection Systems for Discovery Missions, Tech. Rep. TM-110440, NASA, 1997.
[3] D. Olynick, Y.-K. Chen, M. E. Tauber, Aerothermodynamics of the Startdust Sample Return Capsule, Journal of Spacecraft and Rockets 36 (3) (1999) 442–462.
[4] H. Ritter, O. Bayle, Y. Mignot, E. Boulier, P. Portela, J. M. Bouilly, R. Sharda, Ongoing European Developments on Entry Heatshields and TPS Materials, in: 8th International Planetary Probe Workshop, Portsmouth, Virginia, 6-10, June, 2011.
[5] R. J. Sharpe, M. D. Wright, NASA Materials Research for Extreme Conditions, Tech. Rep. TM-2009-215901, NASA, 2009.
[6] B. T. F. Chung, J. Hsiao, Heat Transfer with Ablation in a Finite Slab Subjected to Time-Variant Heat Fluxes, AIAA Journal 23 (1) (1985) 145–150.
[7] T. R. Goodman, Application of Integral Methods to Transient Nonlinear Heat, Advances in Heat Transfer 1 (1964) 51–122.
[8] R. M. Kendall, E. P. Bartlett, R. A. Rindal, C. B. Moyer, An Analysis of the Coupled Chemically Reacting Boundary Layer and Charring Ablator: Part 1, Summary Report, Tech. Rep. CR 1060, NASA, 1968.
[9] S. A. Leone, R. L. Potts, A. L. Laganelli, Enhancements to Integral Solutions to Ablation and Charring, Journal of Spacecraft and Rockets 32 (2) (1995) 210–216.
[10] S. Maruyama, R. Viskanta, T. Aihara, Active Thermal Protection System against Intense Irradiation, Journal of Thermophysics and Heat Transfer 3 (4) (1989) 389–394.
[11] R. L. Potts, Hybrid Integral/Quasi-Steady Solution of Charring Ablation, in: 5th Joint Thermophysics and Heat Transfer Conference, AIAA, doi:10.2514/6.1990-1677, 1990.
[12] R. L. Potts, An Integral Method Theorem for Heat Conduction, AIAA Journal 21 (4) (1983) 630–631.
[13] R. L. Potts, Application of Integral Methods to Ablation Charring Erosion - A Review, Journal of Spacecraft and Rockets 32 (2) (1995) 200–209.
[14] Y. Maisonneuve, Ablation of Solid-Fuel Booster Nozzel Materials, Aerospace Science and Technology 4 (1997) 277–289.
[15] V. Quan, Integral Solution for Erosion Heat Transfer, AIAA Journal 8 (8) (1970) 1512–1514.
[16] G. F. Sykes Jr, Decomposition Characteristics of a Char-Forming Phenolic Polymer Used for Ablative Composites., Tech. Rep. TN D-3810, NASA, 1967.
[17] A. Turchi, D. Bianchi, F. Nasuti, M. Onofri, A Numerical Approach for the Study of the Gas–surface Interaction in Carbon–phenolic Solid Rocket Nozzles, Aerospace Science and Technology 27 (1) (2013) 25–31, ISSN 12709638, doi:10.1016/j.ast.2012.06.003.
[18] J. Lachaud, T. van Eekelen, J. B. Scoggins, T. E. Magin, N. N. Mansour, Detailed Chemical Equilibrium Model for Porous Ablative Materials, International Journal of Heat and Mass Transfer 90 (2015) 1034–1045, ISSN 00179310, doi:10.1016/j.ijheatmasstransfer.2015.05.106.
[19] C. Shao, L. Nie, W. Chen, Analysis of Weakly Ionized Ablation Plasma Flows for a Hypersonic Vehicle, Aerospace Science and Technology 51 (2016) 151–161, ISSN 12709638, doi:10.1016/j.ast.2016.02.005.
[20] D. Bose, J. L. Brown, D. K. Prabhu, P. Gnoffo, C. O. Johnston, B. Hollis, Uncertainty Assessment of Hypersonic Aerothermodynamics Prediction Capability, Journal of Spacecraft and Rockets 50 (1) (2013) 12–18, ISSN 0022-4650, doi:10.2514/1.A32268.
[21] D. Bose, M. Olson, B. Laub, T. White, J. Feldman, J. Santos, M. Mahzari, M. MacLean, A. Dufrene, M. Holden, Initial Assessment of Mars Science Laboratory Heatshield Instrumentation and Flight Data, in: 51st AIAA Aerospace Sciences Meeting Including the New Horizons Forum and Aerospace Exposition, vol. 2013-0908, AIAA, ISBN 978-1-62410-181-6, doi:10.2514/6.2013-908, 2013.
[22] B. R. Hollis, D. K. Prabhu, Assessment of Laminar, Convective Aeroheating Prediction Uncertainties for Mars-Entry Vehicles, Journal of Spacecraft and Rockets 50 (1) (2013) 56–68, ISSN 0022-4650, doi:10.2514/1.A32257.

[23] M. Wright, K. Edquist, C. Tang, B. Hollis, P. Krasa, C. Campbell, A Review of Aerothermal Modeling for Mars Entry Missions, in: 48th AIAA Aerospace Sciences Meeting Including the New Horizons Forum and Aerospace Exposition, AIAA, doi:10.2514/6.2010-443, 2010.
[24] J. Lachaud, N. N. Mansour, Porous-Material Analysis Toolbox Based on OpenFOAM and Applications, Journal of Thermophysics and Heat Transfer 28 (2) (2014) 191–202, ISSN 0887-8722, 1533-6808, doi:10.2514/1.T4262.
[25] F. S. Milos, Y. K. Chen, Comprehensive Model for Multi-Component Ablation Thermochemistry, in: 35th Aerospace Sciences Meeting and Exhibit, vol. 97-0141, AIAA, 1997.
[26] F. S. Milos, Y.-K. Chen, T. Gokcen, Nonequilibrium Ablation of Phenolic Impregnated Carbon Ablator (Milos et Al).Pdf, in: 48th AIAA Aerospace Sciences Meeting Including the New Horizons Forum and Aerospace Exposition, vol. 2010-981, AIAA, 2010.
[27] F. S. Milos, Y.-K. Chen, Ablation, Thermal Response, and Chemistry Program for Analysis of Thermal Protection Systems, Journal of Spacecraft and Rockets 50 (1) (2013) 137–149, doi:10.2514/1.A32302.
[28] C. Park, S.-H. Lee, Validation of Multi-Temperature Nozzle Flow Code NOZNT, in: 28th Therrnophysics Conference, vol. 93–2862, AIAA, 1993.
[29] C. Park, J. T. Howe, R. L. Jaffe, G. V. Candler, Review of Chemical-Kinetic Problems of Future NASA Missions, II: Mars Entries, Journal of Thermophysics and Heat Transfer 8 (1) (1994) 9–23.
[30] C. Park, R. L. Jaffe, H. Partridge, Chemical-Kinetic Parameters of Hyperbolic Earth Entry, Journal of Thermophysics and Heat Transfer 15 (1) (2001) 76–90.
[31] A. Martin, I. Boyd, Non-Darcian Behavior of Pyrolysis Gas in a Thermal Protection System, Journal of Thermophysics and Heat Transfer 24 (1) (2010) 60–68.
[32] H.-W. Wong, J. Peck, R. Edwards, G. Reinisch, J. Lachaud, N. N. Mansour, Measurement of Pyrolysis Products from Phenolic Polymer Thermal Decomposition, in: 52nd Aerospace Sciences Meeting, vol. 2014-1388, AIAA, ISBN 978-1-62410-256-1, doi:10.2514/6.2014-1388, 2014.
[33] H. Weng, S. C. C. Bailey, A. Martin, Numerical Study of Iso-Q Sample Geometric Effects on Charring Ablative Materials, International Journal of Heat and Mass Transfer 80 (2015) 570–596.
[34] P. W. Kopf, Phenolic Resins, in: Encyclopedia of Polymer Science and Technology, vol. 7, John Wiley & Sons, Inc., ISBN 978-0-471-44026-0, 2002.
[35] J. Lachaud, T. E. Magin, I. Cozmuta, N. N. Mansour, A Short Review of Ablative Material Response Models and Simulation Tools, in: 7th European Symposium on the Aerothermodynamics, 9–12, 2011.
[36] B. J. McBride, M. J. Zehe, S. Gordon, NASA Glenn Coefficients for Calculating Thermodynamic Properties of Individual Species, Tech. Rep. 211556, NASA, 2002.
[37] S. Pope, Gibbs Function Continuation for the Stable Computation of Chemical Equilibrium, Combustion and Flame 139 (3) (2004) 222–226, ISSN 00102180, doi:10.1016/j.combustflame.2004.07.008.
[38] J. B. Scoggins, T. E. Magin, Gibbs Function Continuation for Linearly Constrained Multiphase Equilibria, Combustion and Flame 162 (12) (2015) 4514–4522, ISSN 00102180, doi:10.1016/j.combustflame.2015.08.027.
[39] J. D. Anderson, Section 14.6, in: Hypersonic and High-Temperature Gas Dynamics, McGraw-Hill Book Company, 2nd edn., 626–629, 1989.
[40] D. R. Lide, CRC Handbook of Chemistry and Physics, CRC press, 2004.
[41] H. B. Niemann, S. K. Atreya, S. J. Bauer, G. R. Carignan, J. E. Demick, R. L. Frost, D. Gautier, J. A. Haberman, D. N. Harpold, D. M. Hunten, G. Israel, J. I. Lunine, W. T. Kasprzak, T. C. Owen, M. Paulkovich, F. Raulin, E. Raaen, S. H. Way, The Abundances of Constituents of Titan's Atmosphere from the GCMS Instrument on the Huygens Probe, Nature 438 (7069) (2005) 779–784, ISSN 0028-0836, 1476-4679, doi:10.1038/nature04122.
[42] J. Rabinovitch, Advancing EDL Technologies for Future Space Missions: From Ground Testing Facilities to Ablative Heatshields, Ph.D. thesis, California Institute of Technology, 2014.
[43] J. Rabinovitch, V. M. Marx, G. Blanquart, Pyrolysis Gas Composition for a Phenolic Impregnated Carbon Ablator Heatshield, in: 11th AIAA/ASME Joint Thermophysics and Heat Transfer Conference, vol. 2014-2246, ISBN 978-1-62410-281-3, doi:10.2514/6.2014-2246, 2014.
[44] H.-W. Wong, J. Peck, R. E. Bonomi, J. Assif, F. Panerai, G. Reinisch, J. Lachaud, N. N. Mansour, Quantitative Determination of Species Production from Phenol-Formaldehyde Resin Pyrolysis, Polymer Degradation and Stability 112 (2015) 122–131, ISSN 01413910, doi:10.1016/j.polymdegradstab.2014.12.020.
[45] K. A. Trick, T. E. Saliba, Mechanisms of the Pyrolysis of Phenolic Resin in a Carbon/Phenolic Composite, Carbon 33 (11) (1995) 1509–1515.
[46] H.-W. Wong, J. Peck, J. Assif, J. Lachaud, N. N. Mansour, Quantitative Determination of Species Production from the Pyrolysis of the Phenolic Impregnated Carbon Ablator (PICA), in: AIAA Science and Technology Forum and Exposition, vol. 2015-1447, AIAA, 2015.
[47] B. K. Bessire, S. A. Lahankar, T. K. Minton, Pyrolysis of Phenolic Impregnated Carbon Ablator (PICA), ACS Applied Materials & Interfaces 7 (3) (2015) 1383–1395, ISSN 1944-8244, 1944-8252, doi:10.1021/am507816f.
[48] C. Powers, R. Kendall, User's Manual: Aerotherm Chemical Equilibrium (ACE) Computer Program, Tech. Rep., Aerotherm Corp, 1969.
[49] A. Martin, I. Cozmuta, I. D. Boyd, M. J. Wright, Kinetic Rates for Gas Phase Chemistry of Phenolic Based Carbon Ablator Decomposition in Atmospheric Air, Journal of Thermophysics and Heat Transfer 29 (2) (2015) 222–240.
[50] B. J. McBride, S. Gordon, M. J. Reno, Thermodynamic Data for Fifty Reference Elements, Tech. Rep. TP 3287, NASA, 1993.
[51] B. J. McBride, S. Gordon, M. J. Reno, Coefficients for Calculating Thermodynamic and Transport Properties of Individual Species, Tech. Rep. TM 4513, NASA, 1993.

[52] S. Gordon, B. J. McBride, Thermodynamic Data to 20 000 K for Monatomic Gases, Tech. Rep. TP 208523, NASA, 1999.
[53] S. Gordon, B. J. McBride, Computer Program for Calculation of Complex Chemical Equilibrium Compositions and Applications: I. Analysis, Tech. Rep. RP 1311, NASA, 1994.
[54] B. J. McBride, S. Gordon, Computer Program for Calculation of Complex Chemical Equilibrium Compositions and Applicaitons: II. Users Manual and Program Description, Tech. Rep. RP 1311, NASA, 1996.
[55] L. V. Gurvich, I. V. Veyts, C. B. Alcock, Thermodynamic Properties of Individual Substances, Hemisphere Pub. Corp., 4th edn., 1989.
[56] TRC, TRC Thermodynamic Tables, Non-Hydrocarbons and TRC Thermodynamic Tables, Hydrocarbons, extent 2001 (loose-leaf tables with individual dates).
[57] M. W. Chase, National Institute of Standards and Technology (U.S.) (Eds.), {NIST-JANAF} Thermochemical Tables, American Chemical Society: American Institute of Physics for the National Institute of Standards and Technology, Washington, DC : New York, 4th ed edn., ISBN 978-1-56396-831-0 978-1-56396-819-8 978-1-56396-820-4, 1998.
[58] O. V. Dorofeeva, V. P. Novikov, D. B. Neumann, NIST-JANAF Thermochemical Tables. I. Ten Organic Molecules Related to Atmospheric Chemistry, Journal of Physical and Chemical Reference Data 30 (2) (2001) 475–513.
[59] B. Ruscic, R. E. Pinzon, M. L. Morton, G. von Laszevski, S. J. Bittner, S. G. Nijsure, K. A. Amin, M. Minkoff, A. F. Wagner, Introduction to Active Thermochemical Tables: Several "Key" Enthalpies of Formation Revisited, The Journal of Physical Chemistry A 108 (45) (2004) 9979–9997, ISSN 1089-5639, 1520-5215, doi:10.1021/jp047912y.
[60] B. Ruscic, R. E. Pinzon, G. von Laszewski, D. Kodeboyina, A. Burcat, D. Leahy, D. Montoy, A. F. Wagner, Active Thermochemical Tables: Thermochemistry for the 21st Century, Journal of Physics: Conference Series 16 (2005) 561–570.
[61] B. Ruscic, Active Thermochemical Tables (ATcT) Values Based on Ver. 1.112 of the Thermochemical Network, 2013.
[62] A. Burcat, B. Ruscic, Third Millenium Ideal Gas and Condensed Phase Thermochemical Database for Combustion with Updates from Active Thermochemical Tables, Tech. Rep. ANL-05/20, Argonne National Laboratory, 2005.
[63] G. Blanquart, H. Pitsch, Thermochemical Properties of Polycyclic Aromatic Hydrocarbons (PAH) from G3MP2B3 Calculations, The Journal of Physical Chemistry A 111 (28) (2007) 6510–6520.
[64] G. Blanquart, P. Pepiot-Desjardins, H. Pitsch, Chemical Mechanism for High Temperature Combustion of Engine Relevant Fuels with Emphasis on Soot Precursors, Combustion and Flame 156 (3) (2009) 588–607.
[65] K. Narayanaswamy, G. Blanquart, H. Pitsch, A Consistent Chemical Mechanism for Oxidation of Substituted Aromatic Species, Combustion and Flame 157 (10) (2010) 1879–1898.
[66] G. Blanquart, Effects of Spin Contamination on Estimating Bond Dissociation Energies of Polycyclic Aromatic Hydrocarbons, International Journal of Quantum Chemistry 115 (12) (2015) 796–801.
[67] C. F. Goldsmith, G. R. Magoon, W. H. Green, Database of Small Molecule Thermochemistry for Combustion, The Journal of Physical Chemistry A 116 (36) (2012) 9033–9057, ISSN 1089-5639, 1520-5215, doi:10.1021/jp303819e.
[68] D. Weininger, SMILES, a Chemical Language and Information System. 1. Introduction to Methodology and Encoding Rules, Journal of Chemical Information and Modeling 28 (1) (1988) 31–36, ISSN 1549-9596, doi:10.1021/ci00057a005.
[69] D. Weininger, A. Weininger, J. L. Weininger, SMILES. 2. Algorithm for Generation of Unique SMILES Notation, Journal of Chemical Information and Modeling 29 (2) (1989) 97–101, ISSN 1549-9596, doi:10.1021/ci00062a008.
[70] D. Weininger, SMILES. 3. DEPICT. Graphical Depiction of Chemical Structures, Journal of Chemical Information and Modeling 30 (3) (1990) 237–243, ISSN 1549-9596, doi:10.1021/ci00067a005.
[71] A. Kazakov, C. D. Muzny, R. D. Chirico, V. V. Diky, M. Frenkel, Web Thermo Tables: An On-Line Version of the TRC Thermodynamic Tables, Journal of Research of the National Institute of Standards and Technology 113 (4) (2008) 209.
[72] E. E. Bolton, Y. Wang, P. A. Thiessen, S. H. Bryant, PubChem: Integrated Platform of Small Molecules and Biological Activities, in: Annual Reports in Computational Chemistry, vol. 4, Elsevier, ISBN 978-0-444-53250-3, 217–241, 2008.
[73] National Cancer Institute, Chemical Identifier Resolver: https://cactus.nci.nih.gov/chemical/structure .
[74] A. Martin, I. D. Boyd, I. Cozmuta, M. J. Wright, Chemistry Model for Ablating Carbon-Phenolic Material during Atmospheric Re-Entry, in: 48th AIAA Aerospace Sciences Meeting and Exhibit, 2010.
[75] J. B. Scoggins, N. N. Mansour, H. A. Hassan, Development of a Reduced Kinetic Mechanism for PICA Pyrolysis Products, in: 42nd AIAA Thermophysics Conference, vol. 2011-3126, AIAA, 2011.
[76] J. de Mûelenaere, J. Lachaud, N. N. Mansour, T. E. Magin, Stagnation Line Approximation for Ablation Thermochemistry, in: 42nd AIAA Thermophysics Conference, vol. 2011-3616, AIAA, 2011.
[77] M. Frenklach, W. Gardiner, S. Stein, D. Clary, T. Yuan, Mechanism of Soot Formation in Acetylene-Oxygen Mixtures, Combustion Science and Technology 50 (1-3) (1986) 79–115, ISSN 0010-2202, 1563-521X, doi:10.1080/00102208608923927.
[78] G. Blanquart, Chemical and Statistical Soot Modeling, Ph.D. thesis, Stanford University, 2008.